International Journal of Non-Linear Mechanics 53 (2013) 63–74

Contents lists available at SciVerse ScienceDirect

International Journal of Non-Linear Mechanics

journal homepage: www.elsevier.com/locate/nlm

A geometrically non-linear formulation of a three-dimensional beam element for solving large deflection multibody system problems

J.B. Jonker [a,*], J.P. Meijaard [a,b]

[a] Laboratory of Mechanical Automation and Mechatronics, Faculty of Engineering Technology, University of Twente, Enschede, The Netherlands
[b] Olton Engineering Consultancy, Enschede, The Netherlands

ARTICLE INFO

Available online 24 January 2013

Keywords:
Discrete deformation modes
Geometric non-linearity
Large deflection
Second-order theory
Timoshenko beam

ABSTRACT

A beam finite element formulation for large deflection problems in the analysis of flexible multibody systems has been proposed. In this formulation, a set of independent discrete deformation modes are defined for each element which are related to conventional small deflection beam theory in a co-rotational frame. The paper examines the applicability of this formulation for a shear-deformable three-dimensional Timoshenko beam model, in which geometric non-linearities due to large deflections, buckling loads and post-buckling are included. The geometric non-linearities are accounted for by additional second-order terms in the expressions for the deformation modes. Some numerical examples including large deflections are presented and discussed in order to illustrate the influence of these terms on the accuracy and rate of convergence. The influence of these terms on the displacements is small, except for bifurcation points where the load–deflection characteristics change drastically. It is demonstrated, by comparison with available results in the literature, that highly accurate solutions can be obtained with the present beam finite element formulation.

1. Introduction

This paper describes the derivation of a spatial beam element based on the generalized strain formulation proposed by Besseling [5] and some applications in problems involving large deflections of beams. The original field of application in the static analysis and buckling analysis [6–8] has been extended to flexible multibody system dynamics [45], with later modifications including a consistent mass description [23] and a statically consistent inclusion of second-order terms in the definition of the discrete deformation modes [30].

Finite elements for non-linear models of flexible beams in a multibody system analysis can be formulated on the basis of either a one-dimensional continuum description with strain measures expressed in a global inertial reference frame or linear or simplified non-linear curvature and strain–displacement relations in a local co-rotational reference frame. Simo and Vu-Quoc [39,40] developed a non-linear beam theory that is known as geometrically exact (GE) beam theory for finite rotations and deformation. The beam configuration is described with respect to a fixed inertial reference frame. Large deformations are accurately represented as this formulation incorporates finite strain measures which are valid for arbitrary large displacements and rotations; see also Géradin and Cardona [14]. This formulation has the advantage of accounting for non-linear effects due to deformation and, therefore, it can be used to study stability (buckling) and other problems where coupling among axial elongation, bending and torsion deformations and forces are important. A critical question in deriving finite element approximations based on the geometrically exact beam theory is the interpolation of finite rotations, which has to be frame invariant to obtain an objective description [12,35].

To avoid the difficulties associated with the interpolation of finite rotations, so-called rotationless formulations have been developed such as the absolute nodal coordinate formulation (ANCF) developed by Shabana [44,38]. In this finite element formulation, absolute nodal position and slope degrees of freedom are used for the interpolation of the position field of beam elements. The absolute coordinates used allow large deformations and an exact description of rigid body displacements. Furthermore, with absolute nodal coordinates and isoparametric interpolations, constant mass matrices are obtained. However, the use of global positions and slopes as nodal coordinates results in a large number of nodal degrees of freedom. For example, a spatial beam element contains 24 nodal degrees of freedom instead of 12 for a conventional two-node beam element. This formulation also suffers from a number of locking mechanisms [17]. The utility of the additional deformation modes resulting from the larger

* Corresponding author. Tel.: +31 74 376 3699.
E-mail address: j.b.jonker@utwente.nl (J.B. Jonker).

0020-7462/$ - see front matter © 2013 Elsevier Ltd. All rights reserved.
http://dx.doi.org/10.1016/j.ijnonlinmec.2013.01.012

number of nodal coordinates is still a topic of investigation [41,37,42,16,17]. In addition, the absolute nodal coordinate formulation complicates the application of moments and imposed rotations. In another rotationless formulation for three-dimensional beams proposed by Avello and Garica de Jalón [2], natural coordinates (NC) are used to describe the position and orientation of the cross-sections of the beam with respect to an inertial frame.

In the co-rotational (CR) formulation a local or co-rotational frame is attached to each flexible beam element. The motion of the element relative to this frame is due only to the deformation of the element. If the element size is chosen sufficiently small, the deformations may be assumed to be small as well, so linear or simplified non-linear beam theory can be used to compute the elastic displacements without introducing significant errors. Co-rotational finite element formulations for straight beams were first presented by Belytschko and Glaum [4] and have been applied for non-linear dynamic analyses of beam structures by others [20,11,18,32]. Additional references can be found in a review of the co-rotational framework [13]. However, when modelling a flexible multibody system with elastic and rigid bodies, conventional co-rotational formulations treat rigid bodies as elastic bodies with large stiffness. Therefore, they are not able to model rigid body dynamics exactly, yielding a reduced computational efficiency, as is a characteristic of all penalty methods. Another disadvantage is the highly coupled kinetic energy expression in terms of relative displacements and the motion of the co-rotational frame.

Co-rotational formulations bear much resemblance to the natural mode approach of Argyris [1] and the generalized strain formulation proposed by Besseling [5] published in the early 1960s. These two approaches refer to the use of deformation modes, by Argyris termed natural modes, for the description of both deformation and rigid body motion of the element and facilitate the development of a finite element based formulation for rigid–flexible multibody system analysis. The latter finite element description was originally developed for linear problems and extended later on for buckling and post-buckling analysis of frame structures [6–8]. This particular finite element description has been adopted to derive a beam finite element formulation for rigid–flexible multibody system analysis [45,23,30,25]. A distinct feature of this finite element formulation is the definition of independent discrete deformation modes (DDM), which are invariant under arbitrary rigid body motions of the element. This way of finite element discretization forms the algebraic analogue of the continuous field concept for the description of deformations and stresses of deformable bodies. The deformation modes are characterized by deformation coordinates, also called generalized deformations, which are expressed as analytical functions of the nodal coordinates referred to the fixed global coordinate system. The deformation functions include the specification of rigid body motions as displacements for which the generalized deformations are zero. Flexible elements are modelled by allowing non-zero deformations. To describe the dynamics, constitutive equations relating generalized deformations and energetically dual generalized stress resultants have to be specified. The derivation of the element stiffness matrix is based on a discretization of the elastic line of a three-dimensional Timoshenko beam model in a local co-rotational frame, whereas the inertia forces are specified by a discretization of the elastic line in the global inertial frame. This formulation combines the advantages of the inertial frame approach, viz derivation of the inertia forces in terms of absolute nodal velocities and accelerations, and the co-rotational approach, viz application of linear or simplified non-linear beam theories to compute the elastic displacements and stress resultants. Only local elastic displacements and rotations are interpolated, so they are intrinsically objective [12,35]. This results in a simple but efficient non-linear dynamic analysis of flexible beams in a multibody system. With this formulation, large deflection problems can be solved accurately as long as the element size is chosen sufficiently small, such that the generalized deformations remain small and linear relations between generalized stress resultants and generalized deformations are valid.

However, when lateral deflections are finite, geometrical non-linearities due to the magnitude of the elastic displacements and rotations couple the equations governing the axial elongation, bending and torsion deformations. Moreover, if a beam is loaded by relatively large forces in comparison with the buckling load, the beam becomes incapable of carrying additional load because of its tendency to change its configuration. Hence, geometric non-linearities arising from change in configuration are important, both since finite deflections occur and since the beam is loaded by relatively large forces in comparison with the buckling load. These geometrical non-linearities can be accounted for by additional second-order terms in the expressions for the deformation modes, such that the existing linear relations between generalized stress resultants and generalized deformations are retained.

Meijaard [30] adopted a finite-strain description proposed by Besseling [8], which is related to Reissner's finite-strain beam theory [33,34] and derived these second-order terms on the basis of a third-order Taylor expansion of the strain energy. This paper instead presents a direct derivation of these second-order terms by using a vectorial approach. This approach provides a clear insight into the non-linear geometrical effects arising from change in configuration. For two-dimensional beams, Jennings and Visser [22,43] used this approach to compute axial shortening due to bending by assuming the lateral deflection curve of the beam to be cubic. For three-dimensional beams additional non-linear geometric couplings among axial elongation, bending and torsion deformation can be significant. A Taylor series expansion is used to expand the non-linear curvature and strain–displacement equations into a polynomial form of second order. Integrating these equations over the length of the beam using the second moment-area theorem [15] yields the additional second-order terms describing the geometric couplings among the axial elongation, bending and torsion deformations. The effect of the second-order terms on the accuracy and rate of convergence is investigated in several examples, viz large deflection problems for a planar cantilever beam and for a spatial beam curved over 45°, the lateral buckling of a cantilever leaf spring and the eigenfrequencies of a parallel leaf-spring mechanism subject to misalignment.

2. Finite element description

We consider a spatial beam element based on the generalized deformation formulation proposed by Besseling [8] for stability analysis and post-buckling analysis of structures. Van der Werff and Jonker [45] introduced a description including Euler parameters which is more appropriate for computations than the original modified Euler angles in multibody system codes and made possible an implementation in the program SPACAR [24]. A consistent mass formulation was derived in [23,29].

2.1. Element configuration

Fig. 1 shows a section of a spatial beam that is modelled with a finite element. The beam is prismatic and the shear centre, centroid and centre of mass of its cross-sections all coincide.

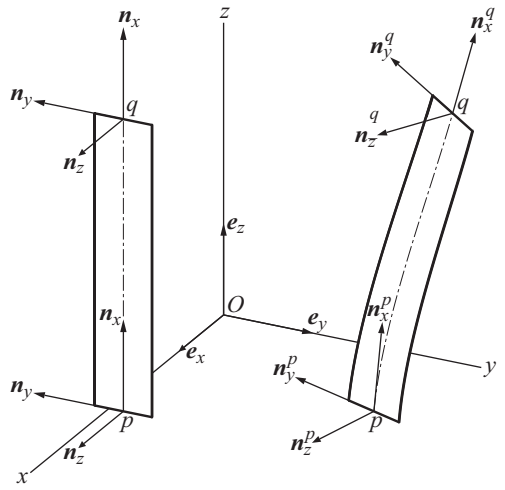

Fig. 1. Spatial beam element, reference and deformed state.

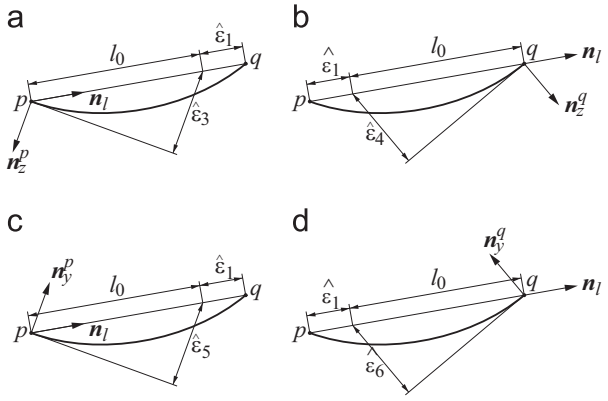

Fig. 2. Bending deformations of the spatial beam element.

The global coordinate system is defined by *Oxyz* with base vectors $\boldsymbol{e}_x$, $\boldsymbol{e}_y$ and $\boldsymbol{e}_z$ pointing along the respective positive directions of the coordinate axes. The configuration of the element is described by the position vectors $\boldsymbol{r}^p$ and $\boldsymbol{r}^q$ at the end nodes p and q, and the angular orientations of the nodes given by triads of unit vectors $(\boldsymbol{n}_x^p,\boldsymbol{n}_y^p,\boldsymbol{n}_z^p)$ and $(\boldsymbol{n}_x^q,\boldsymbol{n}_y^q,\boldsymbol{n}_z^q)$. In the undeflected reference configuration the triads at the nodes coincide and are given by $(\boldsymbol{n}_x,\boldsymbol{n}_y,\boldsymbol{n}_z)$; the unit vector $\boldsymbol{n}_x$ points in the direction of the axis pq and $\boldsymbol{n}_y$ and $\boldsymbol{n}_z$ are in the directions of the principal axes of the cross-section. The rotations of the triads attached to the nodes are described by rotation matrices $\boldsymbol{R}^p$ and $\boldsymbol{R}^q$, so

$$\begin{aligned}&\boldsymbol{n}_x^p=\boldsymbol{R}^p\boldsymbol{n}_x,\quad \boldsymbol{n}_x^q=\boldsymbol{R}^q\boldsymbol{n}_x,\\ &\boldsymbol{n}_y^p=\boldsymbol{R}^p\boldsymbol{n}_y,\quad \boldsymbol{n}_y^q=\boldsymbol{R}^q\boldsymbol{n}_y,\\ &\boldsymbol{n}_z^p=\boldsymbol{R}^p\boldsymbol{n}_z,\quad \boldsymbol{n}_z^q=\boldsymbol{R}^q\boldsymbol{n}_z.\end{aligned}\tag{1}$$

If the beam is rigid then the rotation matrices $\boldsymbol{R}^p$ and $\boldsymbol{R}^q$ are identical and in the initial undeformed state they are equal to the identity matrix. In the present description Euler parameters are used to parametrize the rotation matrices, but the formulation can easily be transformed if a different choice is made. If the Euler parameters are denoted by $(\lambda_0,\boldsymbol{\lambda})$ with the scalar part λ_0 and the vector part $\boldsymbol{\lambda}=(\lambda_1,\lambda_2,\lambda_3)^{\mathrm{T}}$, a rotation matrix can be expressed as [26]

$$\boldsymbol{R}(\lambda_0,\boldsymbol{\lambda})=(\lambda_0^2-\boldsymbol{\lambda}^{\mathrm{T}}\boldsymbol{\lambda})\boldsymbol{I}+2\lambda_0\tilde{\boldsymbol{\lambda}}+2\boldsymbol{\lambda}\boldsymbol{\lambda}^{\mathrm{T}},\tag{2}$$

where use has been made of the tilde notation to denote the skew-symmetric matrix associated with a vector, i.e.

$$\tilde{\boldsymbol{\lambda}}=\begin{bmatrix}0&-\lambda_3&\lambda_2\\ \lambda_3&0&-\lambda_1\\ -\lambda_2&\lambda_1&0\end{bmatrix}.\tag{3}$$

By definition, the Euler parameters must satisfy the constraint equation

$$\lambda_0^2+\boldsymbol{\lambda}^{\mathrm{T}}\boldsymbol{\lambda}=1.\tag{4}$$

2.1.1. Deformation modes

The nodal coordinates of the spatial beam element are the six Cartesian coordinates representing the vectors $\boldsymbol{r}^p$ and $\boldsymbol{r}^q$ and the two sets of Euler parameters $(\lambda_0^p,\boldsymbol{\lambda}^p)$ and $(\lambda_0^q,\boldsymbol{\lambda}^q)$. If a redundant parametrization for the rotations is used, only six of them are independent. Therefore, as the beam has six degrees of freedom as a rigid body and 12 independent nodal coordinates, six independent deformation modes, specified by a set of deformation coordinates $\hat{\varepsilon}_i$, can be chosen, which are expressed as analytical functions of the nodal coordinates x_k, referred to the fixed global coordinate system,

$$\hat{\varepsilon}_i=\hat{\mathcal{D}}_i(x_k),\quad i=1,\ldots,6,\ k=1,\ldots,12\tag{5a}$$

or

$$\hat{\boldsymbol{\varepsilon}}=\hat{\boldsymbol{\mathcal{D}}}(\boldsymbol{x}),\tag{5b}$$

where

$$\boldsymbol{x}=[\boldsymbol{r}^{p\mathrm{T}},(\lambda_0^p,\boldsymbol{\lambda}^{p\mathrm{T}}),\boldsymbol{r}^{q\mathrm{T}},(\lambda_0^q,\boldsymbol{\lambda}^{q\mathrm{T}})]^{\mathrm{T}}.\tag{6}$$

A suitable choice for these deformation functions is [25]

$$\begin{aligned}&\hat{\varepsilon}_1=l-l_0 && \text{(axial elongation)}\\ &\hat{\varepsilon}_2=l_0(\boldsymbol{n}_z^{p\mathrm{T}}\boldsymbol{n}_y^q-\boldsymbol{n}_y^{p\mathrm{T}}\boldsymbol{n}_z^q)/2 && \text{(torsion)}\\ &\left.\begin{aligned}&\hat{\varepsilon}_3=-l_0\boldsymbol{n}_l^{\mathrm{T}}\boldsymbol{n}_z^p,\quad \hat{\varepsilon}_4=l_0\boldsymbol{n}_l^{\mathrm{T}}\boldsymbol{n}_z^q\\ &\hat{\varepsilon}_5=l_0\boldsymbol{n}_l^{\mathrm{T}}\boldsymbol{n}_y^p,\quad \hat{\varepsilon}_6=-l_0\boldsymbol{n}_l^{\mathrm{T}}\boldsymbol{n}_y^q\end{aligned}\right\} && \text{(bending)}\end{aligned}\tag{7}$$

where l_0 is the reference length of the element, $\boldsymbol{l}=\boldsymbol{r}^q-\boldsymbol{r}^p$ is the vector from node p to node q, $l=\|\boldsymbol{l}\|$ is the distance between the nodes and $\boldsymbol{n}_l=(\boldsymbol{r}^q-\boldsymbol{r}^p)/l$ is the unit vector directed from node p to node q. The deformation functions are frame-invariant, which means that they do not change if the element undergoes an arbitrary rigid body motion. The deformation coordinate $\hat{\varepsilon}_1$ describes the axial elongation, $\hat{\varepsilon}_2$ is the torsion and $\hat{\varepsilon}_3$, $\hat{\varepsilon}_4$ and $\hat{\varepsilon}_5$, $\hat{\varepsilon}_6$ are the bending in the *xz*- and *xy*-plane, respectively. The bending deformation modes are visualized in Fig. 2. The deformation coordinates that describe the bending do not change if the beam undergoes an axial elongation with fixed orientations of the nodes and fixed direction $\boldsymbol{n}_l$. The physical dimension of all generalized deformations is length. The deformations of the element can be constrained by imposing conditions on $\hat{\varepsilon}_i$; in particular, the element can be made rigid by imposing the six conditions $\hat{\varepsilon}_i=0$ $(i=1,\ldots,6)$.

2.1.2. Dual stress resultants and equilibrium equations

Let us consider an equilibrium force system defined by the forces $\boldsymbol{F}^p$ and $\boldsymbol{F}^q$ and the moments $\boldsymbol{T}^p$ and $\boldsymbol{T}^q$ applied at the nodal points p and q of the free element, which are placed in a vector of element nodal forces

$$\boldsymbol{F}=[\boldsymbol{F}^{p\mathrm{T}},\boldsymbol{T}^{p\mathrm{T}},\boldsymbol{F}^{q\mathrm{T}},\boldsymbol{T}^{q\mathrm{T}}]^{\mathrm{T}}.\tag{8}$$

Furthermore, we consider virtual variations of the nodal positions, $\delta\boldsymbol{r}^p$ and $\delta\boldsymbol{r}^q$, and virtual rotations, $\delta\boldsymbol{\varphi}^p$ and $\delta\boldsymbol{\varphi}^q$, which are collected in a vector of virtual nodal displacements

$$\delta\boldsymbol{u}=\begin{bmatrix}\delta\boldsymbol{u}^p\\ \delta\boldsymbol{u}^q\end{bmatrix}=[\delta\boldsymbol{r}^{p\mathrm{T}},\ \delta\boldsymbol{\varphi}^{p\mathrm{T}},\ \delta\boldsymbol{r}^{q\mathrm{T}},\ \delta\boldsymbol{\varphi}^{q\mathrm{T}}]^{\mathrm{T}}.\tag{9}$$

The variations $\delta\boldsymbol{\varphi}^p$ and $\delta\boldsymbol{\varphi}^q$ define infinitesimally small rotations from a general configuration with components along the axes of the inertial coordinate system. These are related to the variations of the Euler parameters $(\lambda_0,\boldsymbol{\lambda})$ by a 3×4 transformation matrix $\boldsymbol{\Lambda}$, as

$$\delta\boldsymbol{\varphi} = 2\boldsymbol{\Lambda}\begin{bmatrix}\delta\lambda_0\\ \delta\boldsymbol{\lambda}\end{bmatrix} = 2[-\boldsymbol{\lambda},\ \lambda_0\boldsymbol{I}+\tilde{\boldsymbol{\lambda}}]\begin{bmatrix}\delta\lambda_0\\ \delta\boldsymbol{\lambda}\end{bmatrix}. \tag{10}$$

Because $\delta\boldsymbol{R}^p = \delta\tilde{\boldsymbol{\varphi}}^p\boldsymbol{R}^p$ and $\delta\boldsymbol{R}^q = \delta\tilde{\boldsymbol{\varphi}}^q\boldsymbol{R}^q$, the variations of the unit vectors in Eq. (1) are

$$\begin{aligned}
&\delta\boldsymbol{n}_x^p = \delta\boldsymbol{\varphi}^p\times\boldsymbol{n}_x^p, \quad \delta\boldsymbol{n}_x^q = \delta\boldsymbol{\varphi}^q\times\boldsymbol{n}_x^q,\\
&\delta\boldsymbol{n}_y^p = \delta\boldsymbol{\varphi}^p\times\boldsymbol{n}_y^p, \quad \delta\boldsymbol{n}_y^q = \delta\boldsymbol{\varphi}^q\times\boldsymbol{n}_y^q,\\
&\delta\boldsymbol{n}_z^p = \delta\bar{\boldsymbol{\varphi}}^p\times\boldsymbol{n}_z^p, \quad \delta\boldsymbol{n}_z^q = \delta\boldsymbol{\varphi}^q\times\boldsymbol{n}_z^q.
\end{aligned} \tag{11}$$

The virtual changes in the deformations, $\delta\hat{\boldsymbol{\varepsilon}}$, are related to the virtual displacements $\delta\boldsymbol{u}$ as defined in Eq. (9) by

$$\delta\hat{\boldsymbol{\varepsilon}} = \hat{\boldsymbol{D}}\delta\boldsymbol{u}. \tag{12}$$

The matrix $\hat{\boldsymbol{D}}$ can be determined from the relations (11). For the generalized deformations defined by Eq. (7) the variations can be expressed as

$$\delta\hat{\boldsymbol{\varepsilon}} = [\hat{\boldsymbol{D}}^p,\hat{\boldsymbol{D}}^q]\begin{bmatrix}\delta\boldsymbol{u}^p\\ \delta\boldsymbol{u}^q\end{bmatrix}, \tag{13}$$

where

$$\hat{\boldsymbol{D}}^p = \begin{bmatrix}
-\boldsymbol{n}_l^{\mathrm{T}} & \boldsymbol{0}^{\mathrm{T}}\\
\boldsymbol{0}^{\mathrm{T}} & \frac{l_0}{2}[\boldsymbol{n}_z^p\times\boldsymbol{n}_y^q - \boldsymbol{n}_y^p\times\boldsymbol{n}_z^q]^{\mathrm{T}}\\
\frac{l_0}{l}[\boldsymbol{n}_z^p-(\boldsymbol{n}_l^{\mathrm{T}}\boldsymbol{n}_z^p)\boldsymbol{n}_l]^{\mathrm{T}} & -l_0(\boldsymbol{n}_z^p\times\boldsymbol{n}_l)^{\mathrm{T}}\\
-\frac{l_0}{l}[\boldsymbol{n}_z^q-(\boldsymbol{n}_l^{\mathrm{T}}\boldsymbol{n}_z^q)\boldsymbol{n}_l]^{\mathrm{T}} & \boldsymbol{0}^{\mathrm{T}}\\
-\frac{l_0}{l}[\boldsymbol{n}_y^p-(\boldsymbol{n}_l^{\mathrm{T}}\boldsymbol{n}_y^p)\boldsymbol{n}_l]^{\mathrm{T}} & l_0(\boldsymbol{n}_y^p\times\boldsymbol{n}_l)^{\mathrm{T}}\\
\frac{l_0}{l}[\boldsymbol{n}_y^q-(\boldsymbol{n}_l^{\mathrm{T}}\boldsymbol{n}_y^q)\boldsymbol{n}_l]^{\mathrm{T}} & \boldsymbol{0}^{\mathrm{T}}
\end{bmatrix} \tag{14a}$$

and

$$\hat{\boldsymbol{D}}^q = \begin{bmatrix}
\boldsymbol{n}_l^{\mathrm{T}} & \boldsymbol{0}^{\mathrm{T}}\\
\boldsymbol{0}^{\mathrm{T}} & \frac{l_0}{2}[\boldsymbol{n}_y^q\times\boldsymbol{n}_z^p - \boldsymbol{n}_z^q\times\boldsymbol{n}_y^p]^{\mathrm{T}}\\
-\frac{l_0}{l}[\boldsymbol{n}_z^p-(\boldsymbol{n}_l^{\mathrm{T}}\boldsymbol{n}_z^p)\boldsymbol{n}_l]^{\mathrm{T}} & \boldsymbol{0}^{\mathrm{T}}\\
\frac{l_0}{l}[\boldsymbol{n}_z^q-(\boldsymbol{n}_l^{\mathrm{T}}\boldsymbol{n}_z^q)\boldsymbol{n}_l]^{\mathrm{T}} & l_0(\boldsymbol{n}_z^q\times\boldsymbol{n}_l)^{\mathrm{T}}\\
\frac{l_0}{l}[\boldsymbol{n}_y^p-(\boldsymbol{n}_l^{\mathrm{T}}\boldsymbol{n}_y^p)\boldsymbol{n}_l]^{\mathrm{T}} & \boldsymbol{0}^{\mathrm{T}}\\
-\frac{l_0}{l}[\boldsymbol{n}_y^q-(\boldsymbol{n}_l^{\mathrm{T}}\boldsymbol{n}_y^q)\boldsymbol{n}_l]^{\mathrm{T}} & -l_0(\boldsymbol{n}_y^q\times\boldsymbol{n}_l)^{\mathrm{T}}
\end{bmatrix}. \tag{14b}$$

Generalized stress resultants, $\hat{\boldsymbol{\sigma}}$, are defined to be energetically dual to the generalized deformations $\hat{\boldsymbol{\varepsilon}}$, that is, the virtual work supplied by the generalized stress resultants is $-\hat{\boldsymbol{\sigma}}^{\mathrm{T}}\delta\hat{\boldsymbol{\varepsilon}}$. According to the principle of virtual work, the element will be in a state of equilibrium if

$$\hat{\sigma}_i\delta\hat{\varepsilon}_i = F_k\delta u_k \quad \text{or} \quad \hat{\boldsymbol{\sigma}}^{\mathrm{T}}\delta\hat{\boldsymbol{\varepsilon}} = \boldsymbol{F}^{\mathrm{T}}\delta\boldsymbol{u} \tag{15}$$

holds for all $\delta\boldsymbol{u}$ and $\delta\hat{\boldsymbol{\varepsilon}}$ depending on $\delta\boldsymbol{u}$ by Eq. (12). Substitution of Eq. (12) into Eq. (15) yields with the transpose matrix $\hat{\boldsymbol{D}}^{\mathrm{T}}$

$$\hat{\boldsymbol{D}}^{\mathrm{T}}\hat{\boldsymbol{\sigma}} = \boldsymbol{F}. \tag{16}$$

These are the equilibrium equations formulated in the deformed configuration of the beam element. From these equations, the equilibrium nodal force systems expressed in terms of the generalized stress-resultant components $\hat{\sigma}_i$ are calculated and visualized in Fig. 3(b)–(f). In all cases, perfect equilibrium is obtained for arbitrary large deformations and rigid-body displacements. This is a direct consequence of the invariance of the deformations under rigid body displacements, as the generalized stress resultants have no contribution to the virtual work in Eq. (15) for virtual rigid body displacements.

In order to identify the generalized stress resultant components of a beam element, we consider the undeformed configuration, in which the unit vectors $(\boldsymbol{n}_x^p,\boldsymbol{n}_y^p,\boldsymbol{n}_z^p)$ and $(\boldsymbol{n}_x^q,\boldsymbol{n}_y^q,\boldsymbol{n}_z^q)$ coincide with the global coordinate axes x, y, z as shown in Fig. 3(a).

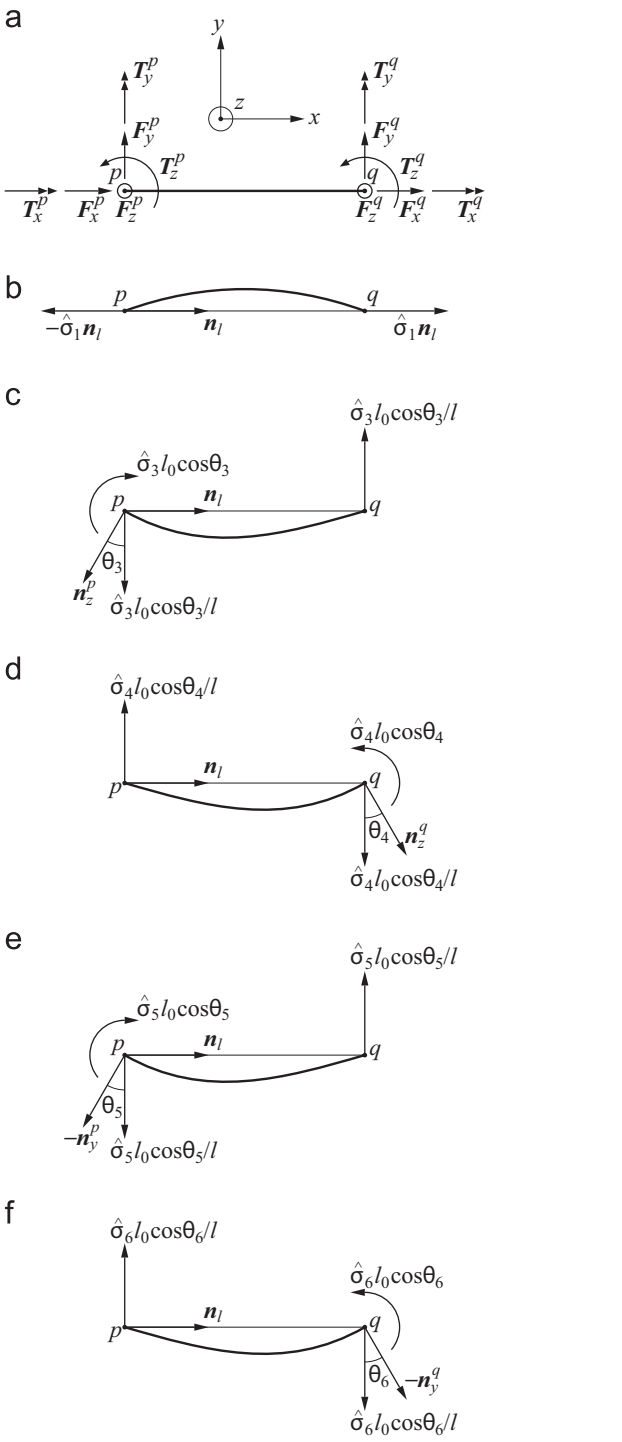

Fig. 3. (a) Equilibrium force system $\boldsymbol{F}$ of nodal forces and moments defined by Eq. (8) and (b)–(f) generalized stress resultants $\hat{\sigma}_1$ and $\hat{\sigma}_3$–$\hat{\sigma}_6$ corresponding to Eq. (16), where $\cos\theta_i = \arcsin(\hat{\varepsilon}_i/l_0)$.

Subsequently, the beam is loaded by an equilibrium force system $\boldsymbol{F}$ defined by Eq. (8). The generalized stress resultant components $\hat{\sigma}_i$ corresponding to the nodal point forces and moments can then be recognized as

$$\left.\begin{aligned}&\hat{\sigma}_1 = -F_x^p = F_x^q \text{ (normal force)}\\ &\hat{\sigma}_2 = -T_x^p/l_0 = T_x^q/l_0 \text{ (twisting moment)}\\ &\hat{\sigma}_3 = -T_y^p/l_0, \quad \hat{\sigma}_4 = T_y^q/l_0\\ &\hat{\sigma}_5 = -T_z^p/l_0, \quad \hat{\sigma}_6 = T_z^q/l_0\end{aligned}\right\} \text{(bending moments)} \tag{17}$$

2.2. Stiffness properties

In this subsection, modified definitions are derived for the deformation modes in which geometrical non-linearities are accounted for by additional second-order terms. The derivation of the element stiffness matrix is based on a discretization of the elastic line of a three-dimensional Timoshenko beam model in a local co-rotational frame.

2.2.1. Description of the elastic line in a co-rotational frame

The elastic line coincides with the centroids of the cross-section, and an orientation is attached to it, describing the rotation of the cross-sections, independent of the tangent to the elastic line. So shear deformations can be described as in Timoshenko's beam theory. A local co-rotational system $\bar{x}$, $\bar{y}$, $\bar{z}$ is introduced with base vectors, $\boldsymbol{e}_{\bar{x}}$, $\boldsymbol{e}_{\bar{y}}$, and $\boldsymbol{e}_{\bar{z}}$ pointing along the respective positive directions of the coordinate axes as shown in Fig. 4. The origin coincides with node p. An overbar denotes a kinematic quantity expressed in the local coordinate system. The $\bar{x}$-axis coincides with the line connecting the nodal points p and q in the current configuration. The $\bar{y}$-axis is chosen in such a way that the unit vector $\boldsymbol{n}_y^p$ lies in the $(\bar{x}, \bar{y})$-plane and the $\bar{z}$-axis completes a right-handed orthogonal system of coordinate axes. In the undeformed reference configuration, $(\boldsymbol{e}_{\bar{x}},\boldsymbol{e}_{\bar{y}},\boldsymbol{e}_{\bar{z}})$ coincide with the unit vectors $(\boldsymbol{n}_x,\boldsymbol{n}_y,\boldsymbol{n}_z)$ in the global frame; $\boldsymbol{e}_{\bar{x}}$ is directed along the centre line and perpendicular to the cross-section, and $\boldsymbol{e}_{\bar{y}}$ and $\boldsymbol{e}_{\bar{z}}$ are directed along the principal axes of the cross-section. The position of point s on the undeformed elastic line with respect to node p is then given by

$$\bar{\boldsymbol{r}}_o = \bar{x}\,\boldsymbol{e}_{\bar{x}}, \quad 0 \le \bar{x} \le l_0, \tag{18}$$

where the coordinate $\bar{x}$ is measured on the straight reference configuration of the beam element, so the coordinate $\bar{x}$ is a material coordinate.

In a deformed configuration, the elastic line moves with the centroids of the cross-sections. If the displacement of the point s is described by a displacement vector $\bar{\boldsymbol{u}}$ with components $(\bar{u}, \bar{v}, \bar{w})$ in the directions of $\boldsymbol{e}_{\bar{x}}$, $\boldsymbol{e}_{\bar{y}}$ and $\boldsymbol{e}_{\bar{z}}$, respectively, the position vector $\bar{\boldsymbol{r}}$ of point s in the deformed configuration can be expressed as

$$\bar{\boldsymbol{r}}(\bar{x}) = \bar{\boldsymbol{r}}_o + \bar{\boldsymbol{u}} = (\bar{x} + \bar{u}(\bar{x}))\boldsymbol{e}_{\bar{x}} + \bar{v}(\bar{x})\boldsymbol{e}_{\bar{y}} + \bar{w}(\bar{x})\boldsymbol{e}_{\bar{z}}. \tag{19}$$

In accordance with the definition of the co-rotational frame, the boundary conditions are

$$\bar{\boldsymbol{r}}(0) = 0, \quad \bar{\boldsymbol{r}}^{\mathrm{T}}(l_0) = [l_0 + \bar{u}^q,\ 0,\ 0], \tag{20}$$

where $\bar{u}^q$ is the axial displacement of point q. The motion of a beam segment can be modelled as a Cosserat rod whose configuration is described by an elastic line $\bar{\boldsymbol{r}}(\bar{x})$ and three orthogonal unit vectors $(\boldsymbol{e}_{\bar{x}}^s,\boldsymbol{e}_{\bar{y}}^s,\boldsymbol{e}_{\bar{z}}^s)$ that describe an average orientation of the cross-section. Note that the unit vector $\boldsymbol{e}_{\bar{x}}^s$ is not tangential to the elastic line in the current configuration, but normal to the cross-section. For a rigid beam, the moving frame $(\boldsymbol{e}_{\bar{x}}^s,\boldsymbol{e}_{\bar{y}}^s,\boldsymbol{e}_{\bar{z}}^s)$ coincides with the co-rotational frame $(\boldsymbol{e}_{\bar{x}},\boldsymbol{e}_{\bar{y}},\boldsymbol{e}_{\bar{z}})$. In general, the orientation of the moving frame is specified by a local rotation matrix $\bar{\boldsymbol{R}}(\bar{x})$ (also called elastic rotation matrix) according to

$$\boldsymbol{e}_{\bar{x}}^s = \bar{\boldsymbol{R}}\boldsymbol{e}_{\bar{x}}, \quad \boldsymbol{e}_{\bar{y}}^s = \bar{\boldsymbol{R}}\boldsymbol{e}_{\bar{y}}, \quad \boldsymbol{e}_{\bar{z}}^s = \bar{\boldsymbol{R}}\boldsymbol{e}_{\bar{z}}. \tag{21}$$

Following Besseling [8], the matrix $\bar{\boldsymbol{R}}$ is defined as the product of three successive rotations about the rotated coordinate axes parametrized by modified Euler angles $(\bar{\varphi}_{\bar{x}},\bar{\varphi}_{\bar{y}},\bar{\varphi}_{\bar{z}})$, also referred to as Tait–Bryan angles, as

$$\bar{\boldsymbol{R}} = \bar{\boldsymbol{R}}(\bar{\varphi}_{\bar{z}})\bar{\boldsymbol{R}}(\bar{\varphi}_{\bar{y}})\bar{\boldsymbol{R}}(\bar{\varphi}_{\bar{x}}), \tag{22}$$

where

$$\bar{\boldsymbol{R}}(\bar{\varphi}_{\bar{x}}) = \begin{bmatrix} 1 & 0 & 0 \\ 0 & \cos\bar{\varphi}_{\bar{x}} & -\sin\bar{\varphi}_{\bar{x}} \\ 0 & \sin\bar{\varphi}_{\bar{x}} & \cos\bar{\varphi}_{\bar{x}} \end{bmatrix}, \tag{23a}$$

$$\bar{\boldsymbol{R}}(\bar{\varphi}_{\bar{y}}) = \begin{bmatrix} \cos\bar{\varphi}_{\bar{y}} & 0 & \sin\bar{\varphi}_{\bar{y}} \\ 0 & 1 & 0 \\ -\sin\bar{\varphi}_{\bar{y}} & 0 & \cos\bar{\varphi}_{\bar{y}} \end{bmatrix}, \tag{23b}$$

$$\bar{\boldsymbol{R}}(\bar{\varphi}_{\bar{z}}) = \begin{bmatrix} \cos\bar{\varphi}_{\bar{z}} & -\sin\bar{\varphi}_{\bar{z}} & 0 \\ \sin\bar{\varphi}_{\bar{z}} & \cos\bar{\varphi}_{\bar{z}} & 0 \\ 0 & 0 & 1 \end{bmatrix}. \tag{23c}$$

In contrast with Euler angles, modified Euler angles avoid singularity problems for small rotations. Another reason for taking modified Euler angles is that for small rotations they may be uniquely defined as components of a rotation vector. The local rotation matrix $\bar{\boldsymbol{R}}$ describes the rotation of a cross-section relative to the local frame due to flexural and torsional deformations of the beam. At the boundary nodes we have

$$\begin{aligned}&\bar{\varphi}_{\bar{x}}(0) = \bar{\varphi}_{\bar{x}}^p = 0, \quad \bar{\varphi}_{\bar{x}}(l_0) = \bar{\varphi}_{\bar{x}}^q,\\ &\bar{\varphi}_{\bar{y}}(0) = \bar{\varphi}_{\bar{y}}^p, \quad \bar{\varphi}_{\bar{y}}(l_0) = \bar{\varphi}_{\bar{y}}^q,\\ &\bar{\varphi}_{\bar{z}}(0) = \bar{\varphi}_{\bar{z}}^p, \quad \bar{\varphi}_{\bar{z}}(l_0) = \bar{\varphi}_{\bar{z}}^q.\end{aligned} \tag{24}$$

The condition on $\bar{\varphi}_{\bar{x}}^p$ implies that the $\bar{y}$-axis is chosen in such a way that the unit vector $\boldsymbol{e}_y^p$ lies in the $(\bar{x},\bar{y})$-plane. The deformed configuration of the beam is now fully determined by the position vector $\bar{\boldsymbol{r}}(\bar{x})$ of the elastic line and the rotation of the moving cross-sectional frame $(\boldsymbol{e}_{\bar{x}}^s,\boldsymbol{e}_{\bar{y}}^s,\boldsymbol{e}_{\bar{z}}^s)$ with respect to the co-rotational frame.

2.2.2. Strain measures

A finite-strain beam theory developed by Reissner [33,34] is adopted to obtain a system of curvature and strain–displacement relations involving axial elongation, shear, torsion and bending curvatures. This finite-strain beam theory forms an extension of the classical Kirchhoff–Love rod theory [27]. The extension

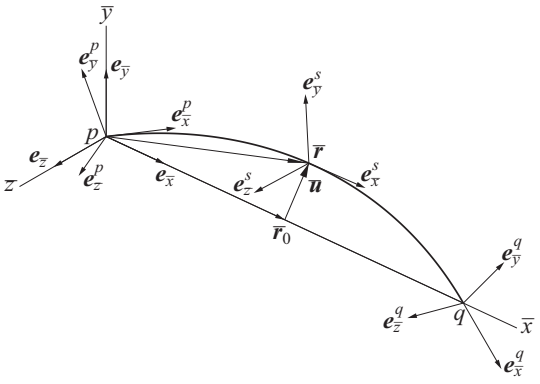

Fig. 4. Configuration of the elastic line in a local, co-rotational, coordinate system.

includes axial elongation and transverse shear of the rod. The same definitions are used by Simo [39] and Avello and Garica de Jalón [2]. Based on the above kinematic description, six independent strains can be defined for each cross-section, one for the axial elongation, two for the transverse shears, one for the torsion and two for the bending in two directions. Reissner defined these as the change of the projections of the derivative of the position of the elastic line with respect to the coordinate $\bar{x}$ and three independent components of the derivative of the local rotation matrix $\bar{\boldsymbol{R}}$ with respect to $\bar{x}$

$$\begin{aligned}&\boldsymbol{\gamma}(\bar{x})=\bar{\boldsymbol{R}}^{\mathrm{T}}\bar{\boldsymbol{r}}'-\boldsymbol{e}_{\bar{x}},\\&\tilde{\boldsymbol{\kappa}}(\bar{x})=\bar{\boldsymbol{R}}^{\mathrm{T}}\bar{\boldsymbol{R}}',\end{aligned}\tag{25}$$

where

$$\boldsymbol{\gamma}=\begin{bmatrix}\gamma_{\bar{x}}\\ \gamma_{\bar{y}}\\ \gamma_{\bar{z}}\end{bmatrix},\quad \tilde{\boldsymbol{\kappa}}=\begin{bmatrix}0 & -\kappa_{\bar{z}} & \kappa_{\bar{y}}\\ \kappa_{\bar{z}} & 0 & -\kappa_{\bar{x}}\\ -\kappa_{\bar{y}} & \kappa_{\bar{x}} & 0\end{bmatrix}.\tag{26}$$

In these expressions, the prime ($'$) denotes differentiation with respect to $\bar{x}$. The strain vector $\boldsymbol{\gamma}(\bar{x})$ represents the axial elongation and two transverse shear strains, and the skew-symmetric matrix $\tilde{\boldsymbol{\kappa}}(\bar{x})$ represents the torsion and two bending curvatures. Written out, the components of $\boldsymbol{\gamma}$ and $\tilde{\boldsymbol{\kappa}}$ are

$$\begin{aligned}&\gamma_{\bar{x}}=\boldsymbol{e}^s_{\bar{x}}\cdot\bar{\boldsymbol{r}}'-1,\quad \kappa_{\bar{x}}=\boldsymbol{e}^s_{\bar{z}}\cdot\boldsymbol{e}^{s\prime}_{\bar{y}},\\&\gamma_{\bar{y}}=\boldsymbol{e}^s_{\bar{y}}\cdot\bar{\boldsymbol{r}}',\quad \kappa_{\bar{y}}=\boldsymbol{e}^s_{\bar{x}}\cdot\boldsymbol{e}^{s\prime}_{\bar{z}},\\&\gamma_{\bar{z}}=\boldsymbol{e}^s_{\bar{z}}\cdot\bar{\boldsymbol{r}}',\quad \kappa_{\bar{z}}=\boldsymbol{e}^s_{\bar{y}}\cdot\boldsymbol{e}^{s\prime}_{\bar{x}}.\end{aligned}\tag{27}$$

The above definitions are the strains defined in [34,39] expressed as functions of the local displacements and rotations. Besseling [8] made a different choice for the strain measuring the axial elongation, namely the Green–Lagrange strain measure, in which the axial strain is just expressed in terms of the first derivative of the vector $\bar{\boldsymbol{r}}$

$$\epsilon_{\bar{x}}=\tfrac{1}{2}(\bar{\boldsymbol{r}}'\cdot\bar{\boldsymbol{r}}'-1).\tag{28}$$

Since the strains are assumed to be small, this choice will not affect the final results. These above strains are invariant under rigid-body displacements. Based on the small deflection assumptions at the level of the co-rotational frame, Taylor series expansions up to second-order can be made for the non-linear curvature and strain–displacement equations. Expanding $\bar{\boldsymbol{R}}$ around the identity matrix up to second-order terms yields

$$\bar{\boldsymbol{R}}=\begin{bmatrix}1-\frac{1}{2}\bar{\varphi}^2_{\bar{y}}-\frac{1}{2}\bar{\varphi}^2_{\bar{z}} & -\bar{\varphi}_{\bar{z}}+\bar{\varphi}_{\bar{x}}\bar{\varphi}_{\bar{y}} & \bar{\varphi}_{\bar{y}}+\bar{\varphi}_{\bar{x}}\bar{\varphi}_{\bar{z}}\\ \bar{\varphi}_{\bar{z}} & 1-\frac{1}{2}\bar{\varphi}^2_{\bar{x}}-\frac{1}{2}\bar{\varphi}^2_{\bar{z}} & -\bar{\varphi}_{\bar{x}}+\bar{\varphi}_{\bar{y}}\bar{\varphi}_{\bar{z}}\\ -\bar{\varphi}_{\bar{y}} & \bar{\varphi}_{\bar{x}} & 1-\frac{1}{2}\bar{\varphi}^2_{\bar{x}}-\frac{1}{2}\bar{\varphi}^2_{\bar{y}}\end{bmatrix}.\tag{29}$$

Using Eqs. (19), (21) and (29), we obtain the a second-order expansion of the non-linear curvature and strain–displacement relations (27), in which $\gamma_{\bar{x}}$ has been replaced by $\epsilon_{\bar{x}}$ from Eq. (28)

$$\epsilon_{\bar{x}}=\bar{u}'+\tfrac{1}{2}(\bar{u}'^2+\bar{v}'^2+\bar{w}'^2),\tag{30a}$$

$$\begin{aligned}&\kappa_{\bar{x}}=\bar{\varphi}'_{\bar{x}}-\bar{\varphi}_{\bar{y}}\bar{\varphi}'_{\bar{z}},\\&\kappa_{\bar{y}}=\bar{\varphi}'_{\bar{y}}+\bar{\varphi}_{\bar{x}}\bar{\varphi}'_{\bar{z}},\end{aligned}\tag{30b}$$

$$\begin{aligned}&\kappa_{\bar{z}}=\bar{\varphi}'_{\bar{z}}-\bar{\varphi}_{\bar{x}}\bar{\varphi}'_{\bar{y}},\\&\gamma_{\bar{y}}=-\bar{\varphi}_{\bar{z}}(1+\bar{u}')+\bar{v}'+\bar{\varphi}_{\bar{x}}(\bar{\varphi}_{\bar{y}}+\bar{w}'),\\&\gamma_{\bar{z}}=\bar{\varphi}_{\bar{y}}(1+\bar{u}')+\bar{w}'-\bar{\varphi}_{\bar{x}}(-\bar{\varphi}_{\bar{z}}+\bar{v}').\end{aligned}\tag{30c}$$

As the longitudinal and transverse shear rigidities are much larger than the flexural and torsional rigidities of a beam, we can neglect the quadratic terms involving the axial displacement $\bar{u}$ and the transverse shear strains $\gamma_{\bar{y}}$ and $\gamma_{\bar{z}}$. When the strains are infinitesimally small, we may neglect the quadratic terms in Eqs. (30), yielding the linearized curvature and strain–displacement relations

$$\epsilon_{\bar{x}}=\bar{u}',\tag{31a}$$

$$\kappa_{\bar{x}}=\bar{\varphi}'_{\bar{x}},\tag{31b}$$

$$\kappa_{\bar{y}}=\bar{\varphi}'_{\bar{y}},\quad \kappa_{\bar{z}}=\bar{\varphi}'_{\bar{z}},\tag{31c}$$

$$\gamma_{\bar{y}}=-\bar{\varphi}_{\bar{z}}+\bar{v}',\quad \gamma_{\bar{z}}=\bar{\varphi}_{\bar{y}}+\bar{w}'.\tag{31d}$$

Eq. (31d) show that due to the inclusion of transverse shear deformation the slopes $\bar{v}'$ and $\bar{w}'$ of the elastic line are not equal to the rotations of the beam's cross-section.

2.2.3. Linearized stiffness formulation

The deformation functions $\hat{\varepsilon}_i$ specified in Eq. (7) can be redefined in the local coordinate system. By making use of the boundary conditions Eq. (20) and by replacing the global unit vectors $\boldsymbol{n}^p_{\bar{y}}$, $\boldsymbol{n}^p_{\bar{z}}$ and $\boldsymbol{n}^q_{\bar{y}}$, $\boldsymbol{n}^q_{\bar{z}}$ by the respective local unit vectors $\boldsymbol{e}^p_{\bar{y}}$, $\boldsymbol{e}^p_{\bar{z}}$ and $\boldsymbol{e}^q_{\bar{y}}$, $\boldsymbol{e}^q_{\bar{z}}$, we obtain

$$\begin{aligned}&\hat{\varepsilon}_1=\bar{u}^q,\\&\hat{\varepsilon}_2=l_0(\boldsymbol{e}^p_{\bar{z}}\cdot\boldsymbol{e}^q_{\bar{y}}-\boldsymbol{e}^p_{\bar{y}}\cdot\boldsymbol{e}^q_{\bar{z}})/2,\\&\hat{\varepsilon}_3=-l_0\boldsymbol{e}_{\bar{x}}\cdot\boldsymbol{e}^p_{\bar{z}},\quad \hat{\varepsilon}_4=l_0\boldsymbol{e}_{\bar{x}}\cdot\boldsymbol{e}^q_{\bar{z}},\\&\hat{\varepsilon}_5=l_0\boldsymbol{e}_{\bar{x}}\cdot\boldsymbol{e}^p_{\bar{y}},\quad \hat{\varepsilon}_6=-l_0\boldsymbol{e}_{\bar{x}}\cdot\boldsymbol{e}^q_{\bar{y}},\end{aligned}\tag{32}$$

where

$$\begin{aligned}&\boldsymbol{e}^p_{\bar{y}}=\bar{\boldsymbol{R}}^p\boldsymbol{e}_{\bar{y}},\quad \boldsymbol{e}^q_{\bar{y}}=\bar{\boldsymbol{R}}^q\boldsymbol{e}_{\bar{y}},\\&\boldsymbol{e}^p_{\bar{z}}=\bar{\boldsymbol{R}}^p\boldsymbol{e}_{\bar{z}},\quad \boldsymbol{e}^q_{\bar{z}}=\bar{\boldsymbol{R}}^q\boldsymbol{e}_{\bar{z}}.\end{aligned}\tag{33}$$

The rotation matrices $\bar{\boldsymbol{R}}^p$ and $\bar{\boldsymbol{R}}^q$ are obtained by evaluating $\bar{\boldsymbol{R}}$ at the nodes p and q. When lateral deflections are assumed to be infinitesimally small, we may neglect the non-linear dependence on the local displacements and rotations in defining the discrete deformation functions. Substituting of Eq. (33) with the second-order rotation matrix $\bar{\boldsymbol{R}}$ of Eq. (29) in Eq. (32), using boundary conditions (24) and disregarding second- and higher-order terms, we obtain the linearized deformations [6]

$$\begin{aligned}&\hat{\varepsilon}_1=\bar{u}^q\quad\text{(axial elongation)}\\&\hat{\varepsilon}_2=l_0\bar{\varphi}^q_{\bar{x}}\quad\text{(torsion)}\\&\left.\begin{aligned}&\hat{\varepsilon}_3=-l_0\bar{\varphi}^p_{\bar{y}},\quad \hat{\varepsilon}_4=l_0\bar{\varphi}^q_{\bar{y}}\\&\hat{\varepsilon}_5=-l_0\bar{\varphi}^p_{\bar{z}},\quad \hat{\varepsilon}_6=l_0\bar{\varphi}^q_{\bar{z}}\end{aligned}\right\}\text{(bending)}\end{aligned}\tag{34}$$

The deformations $\hat{\varepsilon}_i$ may be linearly related to the normal force $\hat{\sigma}_1$, twisting moment $\hat{\sigma}_2$ and four bending moments $\hat{\sigma}_3$, $\hat{\sigma}_4$ and $\hat{\sigma}_5$, $\hat{\sigma}_6$ by a stiffness matrix $\boldsymbol{S}$,

$$\hat{\boldsymbol{\sigma}}=\boldsymbol{S}\hat{\boldsymbol{\varepsilon}},\tag{35}$$

where $\boldsymbol{S}$ is a symmetric block-diagonal matrix containing the elasticity constants

$$\boldsymbol{S}=\mathrm{diag}\{S_1,S_2,\boldsymbol{S}_3,\boldsymbol{S}_4\},\tag{36}$$

with

$$\begin{aligned}&S_1=\frac{EA}{l_0},\quad S_2=\frac{k_{\bar{x}}GI_{\mathrm{p}}}{l_0^3},\\&\boldsymbol{S}_3=\frac{EI_{\bar{y}}}{(1+\Phi_{\bar{z}})l_0^3}\begin{bmatrix}4+\Phi_{\bar{z}} & -2+\Phi_{\bar{z}}\\ -2+\Phi_{\bar{z}} & 4+\Phi_{\bar{z}}\end{bmatrix},\\&\boldsymbol{S}_4=\frac{EI_{\bar{z}}}{(1+\Phi_{\bar{y}})l_0^3}\begin{bmatrix}4+\Phi_{\bar{y}} & -2+\Phi_{\bar{y}}\\ -2+\Phi_{\bar{y}} & 4+\Phi_{\bar{y}}\end{bmatrix}\end{aligned}\tag{37}$$

and shear factors

$$\Phi_{\bar{z}}=\frac{12EI_{\bar{y}}}{k_{\bar{z}}GAl_0^2},\quad \Phi_{\bar{y}}=\frac{12EI_{\bar{z}}}{k_{\bar{y}}GAl_0^2}.\tag{38}$$

Here, E is the modulus of elasticity (Young's modulus), G is the shear modulus, A is the area of the cross-section, I_p the polar moment of inertia, $k_{\bar{x}}$ is the torsion correction factor according to Saint–Venant's theory, $I_{\bar{y}}$ and $I_{\bar{z}}$ are the moments of inertia of the cross-section with respect to the principal axes, and $k_{\bar{y}}$ and $k_{\bar{z}}$ are shear correction coefficients according to Cowper [10] that account for the non-uniform distribution of the shear stress over the beam's cross-section. The derivation of the elasticity constants and the elastic displacement and rotation components is based on the exact solution of the equilibrium equations of the three-dimensional Timoshenko beam for the case when the beam is loaded by equilibrium forces and moments at its nodes. The elastic displacement vector $\bar{\boldsymbol{u}}(\xi)$ of an arbitrary point with coordinate $\bar{x}=\xi l_0$ can be expressed as a vectorial sum of a axial and lateral displacements, i.e. in the form of Eq. (19)

$$\begin{aligned}\bar{\boldsymbol{u}}(\xi)&=\bar{u}(\xi)\boldsymbol{e}_{\bar{x}}+\bar{v}(\xi)\boldsymbol{e}_{\bar{y}}+\bar{w}(\xi)\boldsymbol{e}_{\bar{z}}\\&=\bar{u}^q u(\xi)\,\boldsymbol{e}_{\bar{x}}+[-l_0\bar{\varphi}_{\bar{z}}^p\;\; l_0\bar{\varphi}_{\bar{z}}^q]\begin{bmatrix}v^p(\xi)\\v^q(\xi)\end{bmatrix}\boldsymbol{e}_{\bar{y}}\\&\quad+[-l_0\bar{\varphi}_{\bar{y}}^p\;\; l_0\bar{\varphi}_{\bar{y}}^q]\begin{bmatrix}w^p(\xi)\\w^q(\xi)\end{bmatrix}\boldsymbol{e}_{\bar{z}}.\end{aligned}\tag{39a}$$

In accordance with the boundary conditions of Eq. (20) we obtain

$$\begin{aligned}u(\xi)&=\xi,\\v^p(\xi)&=-\frac{1}{1+\Phi_{\bar{y}}}\left[\xi^3-2\xi^2+\xi+\frac{1}{2}\Phi_{\bar{y}}(-\xi^2+\xi)\right],\\v^q(\xi)&=-\frac{1}{1+\Phi_{\bar{y}}}\left[-\xi^3+\xi^2+\frac{1}{2}\Phi_{\bar{y}}(-\xi^2+\xi)\right],\\w^p(\xi)&=\frac{1}{1+\Phi_{\bar{z}}}\left[\xi^3-2\xi^2+\xi+\frac{1}{2}\Phi_{\bar{z}}(-\xi^2+\xi)\right],\\w^q(\xi)&=\frac{1}{1+\Phi_{\bar{z}}}\left[-\xi^3+\xi^2+\frac{1}{2}\Phi_{\bar{z}}(-\xi^2+\xi)\right].\end{aligned}\tag{39b}$$

The rotation vector $\bar{\boldsymbol{\varphi}}$ can be written as

$$\begin{aligned}l_0\bar{\boldsymbol{\varphi}}(\xi)&=l_0\bar{\varphi}_{\bar{x}}(\xi)\,\boldsymbol{e}_{\bar{x}}+l_0\bar{\varphi}_{\bar{y}}(\xi)\boldsymbol{e}_{\bar{y}}+l_0\bar{\varphi}_{\bar{z}}(\xi)\boldsymbol{e}_{\bar{z}}\\&=l_0\bar{\varphi}_{\bar{x}}^q\phi_{\bar{x}}(\xi)\boldsymbol{e}_{\bar{x}}+[-l_0\bar{\varphi}_{\bar{y}}^p\;\; l_0\bar{\varphi}_{\bar{y}}^q]\begin{bmatrix}\phi_{\bar{y}}^p(\xi)\\\phi_{\bar{y}}^q(\xi)\end{bmatrix}\boldsymbol{e}_{\bar{y}}\\&\quad+[-l_0\bar{\varphi}_{\bar{z}}^p\;\; l_0\bar{\varphi}_{\bar{z}}^q]\begin{bmatrix}\phi_{\bar{z}}^p(\xi)\\\phi_{\bar{z}}^q(\xi)\end{bmatrix}\boldsymbol{e}_{\bar{z}}.\end{aligned}\tag{40a}$$

and with the boundary conditions (24) the shape functions become

$$\begin{aligned}\phi_{\bar{x}}(\xi)&=\xi,\\\phi_{\bar{y}}^p(\xi)&=\frac{1}{1+\Phi_{\bar{z}}}[-3\xi^2+4\xi-1+\Phi_{\bar{z}}(\xi-1)],\\\phi_{\bar{y}}^q(\xi)&=\frac{1}{1+\Phi_{\bar{z}}}[3\xi^2-2\xi+\Phi_{\bar{z}}\xi],\\\phi_{\bar{z}}^p(\xi)&=\frac{1}{1+\Phi_{\bar{y}}}[-3\xi^2+4\xi-1+\Phi_{\bar{y}}(\xi-1)],\\\phi_{\bar{z}}^q(\xi)&=\frac{1}{1+\Phi_{\bar{y}}}[3\xi^2-2\xi+\Phi_{\bar{y}}\xi].\end{aligned}\tag{40b}$$

The shape functions $w^p(\xi)$, $w^q(\xi)$, $v^p(\xi)$ and $v^q(\xi)$ are the conventional cubic Hermite polynomials with additional terms containing the shear factors that account for the effects of shear. The shape functions for the axial elongation $\bar{u}(\xi)$ and the twist angle $\bar{\varphi}_{\bar{x}}(\xi)$ are included for the sake of completeness.

2.2.4. Consistency verification

With the elastic shape functions for the axial and torsional deformation, the axial elongation $\hat{\varepsilon}_1$ and torsional deformation $\hat{\varepsilon}_2$ can be evaluated. Substituting for $\bar{u}(\xi)$ and $l_0\bar{\varphi}_{\bar{x}}(\xi)$ from Eqs. (39a) and (40a) into the linearized curvature and strain–displacement relations of Eqs. (31a) and (31b) and integrating over the length of the beam, we obtain

$$\int_0^{l_0}\epsilon_{\bar{x}}\,\mathrm{d}\bar{x}=\int_0^1\bar{u}'\,\mathrm{d}\xi=\bar{u}^q=\hat{\varepsilon}_1,\tag{41a}$$

$$l_0\int_0^{l_0}\kappa_{\bar{x}}\,\mathrm{d}\bar{x}=l_0\int_0^1\bar{\varphi}_{\bar{x}}'\,\mathrm{d}\xi=l_0\bar{\varphi}_{\bar{x}}^q=\hat{\varepsilon}_2.\tag{41b}$$

In these expressions and further on, the prime ($'$) denotes differentiation with respect to ξ. Expressions for the bending deformations $\hat{\varepsilon}_3$–$\hat{\varepsilon}_6$ can be obtained from the second moment-area theorem [15], including the effects of transverse shear deformation. Substituting for $\bar{\varphi}_{\bar{y}}(\xi)$, $\bar{\varphi}_{\bar{z}}(\xi)$ and $\bar{v}(\xi)$, $\bar{w}(\xi)$ from Eqs. (40a) and (39a) into Eqs. (31c) and (31d), applying the theorem and neglecting second- and higher-order terms we obtain

$$\begin{aligned}\int_0^{l_0}[\kappa_{\bar{y}}(l_0-\bar{x})-\gamma_{\bar{z}}]\,\mathrm{d}\bar{x}&=l_0\int_0^1\left[\bar{\varphi}_{\bar{y}}'(1-\xi)-\left(\bar{\varphi}_{\bar{y}}+\frac{1}{l_0}\bar{w}'\right)\right]\mathrm{d}\xi\\&=-l_0\,\bar{\varphi}_{\bar{y}}^p=\hat{\varepsilon}_3,\end{aligned}\tag{42a}$$

$$\int_0^{l_0}[\kappa_{\bar{y}}\bar{x}+\gamma_{\bar{z}}]\,\mathrm{d}\bar{x}=l_0\int_0^1\left[\bar{\varphi}_{\bar{y}}'\xi+\bar{\varphi}_{\bar{y}}+\frac{1}{l_0}\bar{w}'\right]\mathrm{d}\xi=l_0\bar{\varphi}_{\bar{y}}^q=\hat{\varepsilon}_4,\tag{42b}$$

$$\begin{aligned}\int_0^{l_0}[\kappa_{\bar{z}}(l_0-\bar{x})+\gamma_{\bar{y}}]\,\mathrm{d}\bar{x}&=l_0\int_0^1\left[\bar{\varphi}_{\bar{z}}'(1-\xi)+\left(-\bar{\varphi}_{\bar{z}}+\frac{1}{l_0}\bar{v}'\right)\right]\mathrm{d}\xi\\&=-l_0\,\bar{\varphi}_{\bar{z}}^p=\hat{\varepsilon}_5,\end{aligned}\tag{42c}$$

$$\int_0^{l_0}[\kappa_{\bar{z}}\,\bar{x}-\gamma_{\bar{y}}]\,\mathrm{d}\bar{x}=l_0\int_0^1\left[\bar{\varphi}_{\bar{z}}'\xi-\left(-\bar{\varphi}_{\bar{z}}+\frac{1}{l_0}\bar{v}'\right)\right]\mathrm{d}\xi=l_0\bar{\varphi}_{\bar{z}}^q=\hat{\varepsilon}_6.\tag{42d}$$

2.2.5. Second-order stiffness formulation

In this section, expressions for the second-order terms are derived through the integration of the non-linear curvature and strain–displacement relations (30) over the length of the beam. Substitution of Eq. (33) with the second-order rotation matrix $\bar{\boldsymbol{R}}$ of Eq. (29) into Eq. (32), using boundary conditions (24) and disregarding third- and higher-order terms we obtain the second-order approximations

$$\begin{aligned}\hat{\varepsilon}_2&=l_0\bar{\varphi}_{\bar{x}}^q+\frac{1}{2l_0}(\hat{\varepsilon}_3-\hat{\varepsilon}_4)(\hat{\varepsilon}_5+\hat{\varepsilon}_6),\\\hat{\varepsilon}_3&=-l_0\bar{\varphi}_{\bar{y}}^p,\\\hat{\varepsilon}_4&=l_0\bar{\varphi}_{\bar{y}}^q+\frac{1}{l_0}\hat{\varepsilon}_2\hat{\varepsilon}_6,\\\hat{\varepsilon}_5&=-l_0\bar{\varphi}_{\bar{z}}^p,\\\hat{\varepsilon}_6&=l_0\bar{\varphi}_{\bar{z}}^q-\frac{1}{l_0}\hat{\varepsilon}_2\hat{\varepsilon}_4.\end{aligned}\tag{43}$$

The quadratic expressions in terms of the torsion and bending deformations originate from the additional non-linearity due to the relative rotations of the unit vectors $\boldsymbol{e}_{\bar{y}}^p$, $\boldsymbol{e}_{\bar{z}}^p$ and $\boldsymbol{e}_{\bar{y}}^q$, $\boldsymbol{e}_{\bar{y}}^q$ attached at the nodal points p and q. Substituting for $l_0\bar{\varphi}_{\bar{x}}^q$, $l_0\bar{\varphi}_{\bar{y}}^p$, $l_0\bar{\varphi}_{\bar{y}}^q$ and $l_0\bar{\varphi}_{\bar{z}}^p$, $l_0\bar{\varphi}_{\bar{z}}^q$ from Eq. (43) into Eqs. (39a) and (40a) yields a second-order approximation of the displacement and rotation fields in terms of the deformation coordinates $\hat{\varepsilon}_i$

$$\begin{aligned}\bar{\boldsymbol{u}}(\xi)&=\bar{u}(\xi)\boldsymbol{e}_{\bar{x}}+\bar{v}(\xi)\boldsymbol{e}_{\bar{y}}+\bar{w}(\xi)\boldsymbol{e}_{\bar{z}}\\&=\hat{\varepsilon}_1 u(\xi)\boldsymbol{e}_{\bar{x}}+\left[\hat{\varepsilon}_5 v^p(\xi)+\left(\hat{\varepsilon}_6+\frac{1}{l_0}\hat{\varepsilon}_2\hat{\varepsilon}_4\right)v^q(\xi)\right]\boldsymbol{e}_{\bar{y}}\\&\quad+\left[\hat{\varepsilon}_3 w^p(\xi)+\left(\hat{\varepsilon}_4-\frac{1}{l_0}\hat{\varepsilon}_2\hat{\varepsilon}_6\right)w^q(\xi)\right]\boldsymbol{e}_{\bar{z}},\end{aligned}\tag{44a}$$

$$\begin{aligned}l_0\bar{\boldsymbol{\varphi}}(\xi)&=l_0\bar{\varphi}_{\bar{x}}(\xi)\boldsymbol{e}_{\bar{x}}+l_0\bar{\varphi}_{\bar{y}}(\xi)\boldsymbol{e}_{\bar{y}}+l_0\bar{\varphi}_{\bar{z}}(\xi)\boldsymbol{e}_{\bar{z}}\\&=\left[\hat{\varepsilon}_2-\frac{1}{2l_0}(\hat{\varepsilon}_3-\hat{\varepsilon}_4)(\hat{\varepsilon}_5+\hat{\varepsilon}_6)\right]\phi_{\bar{x}}(\xi)\boldsymbol{e}_{\bar{x}}\end{aligned}$$

$$+\left[\hat{\varepsilon}_3\phi_{\bar{y}}^p(\xi)+\left(\hat{\varepsilon}_4-\frac{1}{l_0}\hat{\varepsilon}_2\hat{\varepsilon}_6\right)\phi_{\bar{y}}^q(\xi)\right]\boldsymbol{e}_{\bar{y}}$$
$$+\left[\hat{\varepsilon}_5\phi_{\bar{z}}^p(\xi)+\left(\hat{\varepsilon}_6+\frac{1}{l_0}\hat{\varepsilon}_2\hat{\varepsilon}_4\right)\phi_{\bar{z}}^q(\xi)\right]\boldsymbol{e}_{\bar{z}}. \tag{44b}$$

Integrating Eq. (30a) over the length of the beam, we obtain a non-linear relation for the axial elongation ε_1 corresponding to the combined second-order displacement distributions $\bar{u}(\xi)$, $\bar{v}(\xi)$ and $\bar{w}(\xi)$

$$\varepsilon_1=\int_0^{l_0}\epsilon_{\bar{x}}\,\mathrm{d}\bar{x}=\int_0^1\bar{u}'\,\mathrm{d}\xi+\frac{1}{2l_0}\int_0^1(\bar{v}'^2+\bar{w}'^2)\,\mathrm{d}\xi. \tag{45}$$

The second-order terms on the right-hand side represent the so-called foreshortening effect [6]. In a similar way, coupling between torsion and bending deformations can be accounted for through integration of Eq. (30b)

$$\varepsilon_2=l_0\int_0^{l_0}\kappa_{\bar{x}}\,\mathrm{d}\bar{x}=l_0\int_0^1(\bar{\varphi}_{\bar{x}}'-\bar{\varphi}_{\bar{y}}\bar{\varphi}_{\bar{z}}')\,\mathrm{d}\xi. \tag{46}$$

The second-order terms on the right-hand side represent the extra torsion of the beam caused by its bending. Expressions representing the coupling between bending and torsion deformations can be obtained from the moment-area theorem [15], including the effects of transverse shear deformation. Using the non-linear curvature and strain–displacement relations of Eqs. (30b) and (30c), we obtain

$$\varepsilon_3=\int_0^{l_0}[\kappa_{\bar{y}}(l_0-\bar{x})-\gamma_{\bar{z}}]\,\mathrm{d}\bar{x}$$
$$=l_0\int_0^1\left[(\bar{\varphi}_{\bar{y}}'+\bar{\varphi}_{\bar{x}}\bar{\varphi}_{\bar{z}}')(1-\xi)-\left(\bar{\varphi}_{\bar{y}}+\frac{1}{l_0}\bar{w}'\right)\right]\mathrm{d}\xi, \tag{47a}$$

$$\varepsilon_4=\int_0^{l_0}[\kappa_{\bar{y}}\bar{x}+\gamma_{\bar{z}}]\,\mathrm{d}\bar{x}$$
$$=l_0\int_0^1\left[(\bar{\varphi}_{\bar{y}}'+\bar{\varphi}_{\bar{x}}\bar{\varphi}_{\bar{z}}')\xi+\left(\bar{\varphi}_{\bar{y}}+\frac{1}{l_0}\bar{w}'\right)\right]\mathrm{d}\xi, \tag{47b}$$

$$\varepsilon_5=\int_0^{l_0}[\kappa_{\bar{z}}(l_0-\bar{x})+\gamma_{\bar{y}}]\,\mathrm{d}\bar{x}$$
$$=l_0\int_0^1\left[(\bar{\varphi}_{\bar{z}}'-\bar{\varphi}_{\bar{x}}\bar{\varphi}_{\bar{y}}')(1-\xi)+\left(-\bar{\varphi}_{\bar{z}}+\frac{1}{l_0}\bar{v}'\right)\right]\mathrm{d}\xi, \tag{47c}$$

$$\varepsilon_6=\int_0^{l_0}[\kappa_{\bar{z}}\bar{x}-\gamma_{\bar{y}}]\,\mathrm{d}\bar{x}$$
$$=l_0\int_0^1\left[(\bar{\varphi}_{\bar{z}}'-\bar{\varphi}_{\bar{x}}\bar{\varphi}_{\bar{y}}')\xi-\left(-\bar{\varphi}_{\bar{z}}+\frac{1}{l_0}\bar{v}'\right)\right]\mathrm{d}\xi. \tag{47d}$$

Substituting the expressions for the derivatives $\bar{u}'(\xi)$, $\bar{v}'(\xi)$ and $\bar{w}'(\xi)$ obtained from Eq. (44a) and for $\bar{\varphi}_{\bar{x}}(\xi)$, $\bar{\varphi}_{\bar{y}}(\xi)$, $\bar{\varphi}_{\bar{z}}(\xi)$ and $\bar{\varphi}_{\bar{x}}'(\xi)$, $\bar{\varphi}_{\bar{y}}'(\xi)$, $\bar{\varphi}_{\bar{z}}'(\xi)$ obtained from Eq. (44b) into Eqs. (45)–(47)and neglecting third- and higher-order terms, we obtain the modified deformations including second-order coupling terms

$$\boldsymbol{\varepsilon}=\mathcal{D}(\boldsymbol{x}), \tag{48a}$$

where

$$\varepsilon_1=\hat{\varepsilon}_1+\frac{1}{30l_0}(2\hat{\varepsilon}_3^2+\hat{\varepsilon}_3\hat{\varepsilon}_4+2\hat{\varepsilon}_4^2+2\hat{\varepsilon}_5^2+\hat{\varepsilon}_5\hat{\varepsilon}_6+2\hat{\varepsilon}_6^2),$$
$$\varepsilon_2=\hat{\varepsilon}_2+\frac{1}{l_0}(-\hat{\varepsilon}_3\hat{\varepsilon}_6+\hat{\varepsilon}_4\hat{\varepsilon}_5),$$
$$\varepsilon_3=\hat{\varepsilon}_3+\frac{1}{6l_0}\hat{\varepsilon}_2(\hat{\varepsilon}_5+\hat{\varepsilon}_6),$$
$$\varepsilon_4=\hat{\varepsilon}_4-\frac{1}{6l_0}\hat{\varepsilon}_2(\hat{\varepsilon}_5+\hat{\varepsilon}_6),$$
$$\varepsilon_5=\hat{\varepsilon}_5-\frac{1}{6l_0}\hat{\varepsilon}_2(\hat{\varepsilon}_3+\hat{\varepsilon}_4),$$
$$\varepsilon_6=\hat{\varepsilon}_6+\frac{1}{6l_0}\hat{\varepsilon}_2(\hat{\varepsilon}_3+\hat{\varepsilon}_4). \tag{48b}$$

These equations are identical to those derived by Meijaard [30]. The second-order terms describe the geometric couplings among the axial elongation, bending and torsion deformations. Note that the integrals in Eqs. (45)–(47) are evaluated analytically using the shape functions (39b) and (40b) of the linear beam model. Because the rigidity against axial elongation is much larger than the flexural and torsional rigidity, the modification for ε_1 is the most important one and the other modifications are only relevant to more special cases. The additional terms in the expressions for the bending deformations take into account the effect of unsymmetrical bending caused by a torsional deformation of the beam. For instance for beams with a small torsional rigidity and a large difference in flexural rigidities (e.g. leaf springs), the mutual influences of lateral deflection and torsional deformation of the beam should be taken into account. With the inclusion of the second-order terms in the definitions of the generalized deformations, the linear relation between generalized deformations $\boldsymbol{\varepsilon}$ and associated stress resultants $\boldsymbol{\sigma}$, as it is reflected in Eq. (35), is retained and still independent of the magnitude of the elastic displacements and rotations.

3. Equations of motion

The equations of motion are derived using d'Alembert's principle, which states that the balance of virtual work

$$\boldsymbol{\sigma}^{\mathrm{T}}\delta\boldsymbol{\varepsilon}=\boldsymbol{F}^{\mathrm{T}}\delta\boldsymbol{u}-\rho Al_0\int_0^1\delta\boldsymbol{r}^{\mathrm{T}}\ddot{\boldsymbol{r}}\,\mathrm{d}\xi, \tag{49}$$

holds for all $\delta\boldsymbol{r}$, $\delta\boldsymbol{u}$ and $\delta\boldsymbol{\varepsilon}$ depending on the variations of the nodal coordinates $\delta\boldsymbol{x}$. The virtual nodal displacements $\delta\boldsymbol{u}$ are related to the virtual variations of the nodal coordinates $\delta\boldsymbol{x}$ by a transformation matrix $\boldsymbol{A}$

$$\delta u_k=A_{kl}\delta x_l \quad\text{or}\quad \delta\boldsymbol{u}=\boldsymbol{A}\delta\boldsymbol{x}, \tag{50}$$

where $\boldsymbol{A}$ is a block-diagonal transformation matrix

$$\boldsymbol{A}=\mathrm{diag}\{\boldsymbol{I},\ 2\boldsymbol{\Lambda}^p,\ \boldsymbol{I},\ 2\boldsymbol{\Lambda}^q\}, \tag{51}$$

where matrix $\boldsymbol{\Lambda}$ has been defined in Eq. (10). Virtual variations of the generalized deformations $\delta\boldsymbol{\varepsilon}$ depend on the virtual variations of the nodal coordinates $\delta\boldsymbol{x}$ through the definition of the deformation functions (48) as

$$\delta\varepsilon_i=\mathcal{D}_{i,k}\delta x_k \quad\text{or}\quad \delta\boldsymbol{\varepsilon}=\boldsymbol{\mathcal{D}}_{,\boldsymbol{x}}\delta\boldsymbol{x}, \tag{52}$$

with

$$\mathcal{D}_{i,k}=\frac{\partial\hat{\mathcal{D}}_i}{\partial\hat{x}_k}\quad\text{and}\quad\boldsymbol{\mathcal{D}}_{,\boldsymbol{x}}=\frac{\partial\boldsymbol{\mathcal{D}}}{\partial\boldsymbol{x}}. \tag{53}$$

The last term represents the virtual work due to the inertia forces, where $\boldsymbol{r}(\xi)$ is the position vector of an infinitesimal particle with mass $\rho Al_0\,\mathrm{d}\xi$. Evaluation of the integral results in

$$-\rho Al_0\int_0^1\delta\boldsymbol{r}^{\mathrm{T}}\ddot{\boldsymbol{r}}\,\mathrm{d}\xi=-\delta\boldsymbol{x}^{\mathrm{T}}[\boldsymbol{M}\ddot{\boldsymbol{x}}+\boldsymbol{h}], \tag{54}$$

where $\boldsymbol{M}(\boldsymbol{x})$ is a position-dependent consistent mass matrix and $\boldsymbol{h}(\boldsymbol{x},\dot{\boldsymbol{x}})$ is a convective inertia term being a quadratic function of velocities. Substitution of Eq. (54) into Eq. (49) yields, with the compatibility equations (50) and (52),

$$\boldsymbol{\mathcal{D}}_{,\boldsymbol{x}}^{\mathrm{T}}\boldsymbol{\sigma}=\boldsymbol{A}^{\mathrm{T}}\boldsymbol{F}-[\boldsymbol{M}\ddot{\boldsymbol{x}}+\boldsymbol{h}]. \tag{55}$$

Eq. (55) are the equations of motion for a free flexible beam element.

3.1. Description of the elastic line in a global frame

In order to derive the mass matrix and the corresponding convective inertia vector, an interpolation of the global position of the elastic line has to be made. The global position vector $\boldsymbol{r}(\xi)$ for a point with material coordinate $\bar{x}=\xi l_0$ in the straight reference configuration of the beam can be expressed as a vectorial sum of a point on the line connecting the nodes and the lateral deflection expressed as the linear combination of four components linear in the deformation coordinates ε_3, ε_4, ε_5 and ε_6, respectively [23], as

$$\begin{aligned}\boldsymbol{r}(\xi)=&(1-\xi)\boldsymbol{r}^p+\xi\boldsymbol{r}^q+\hat{\varepsilon}_3 w^p(\xi)\boldsymbol{n}_z^p+\hat{\varepsilon}_4 w^q(\xi)\boldsymbol{n}_z^q\\&+\hat{\varepsilon}_5 v^p(\xi)\boldsymbol{n}_y^p+\hat{\varepsilon}_6 v^q(\xi)\boldsymbol{n}_y^q,\end{aligned}\tag{56}$$

where the shape functions $w^p(\xi)$, $w^q(\xi)$, $v^p(\xi)$ and $v^q(\xi)$ are defined by Eq. (39b). Eq. (56) shows that the displacement field associated with the bending deformation of the beam is described with respect to four co-rotational frames that coincide with the unit vectors $\boldsymbol{n}_y^p$, $\boldsymbol{n}_z^p$ and $\boldsymbol{n}_y^q$, $\boldsymbol{n}_z^q$ at the nodes p and q. Since the deformations are assumed to be small, Eq. (56) can be approximated by a Hermite interpolation for the elastic line [29], in which case the global position vector $\boldsymbol{r}(\xi)$ can be expressed as

$$\begin{aligned}\boldsymbol{r}(\xi)=&(2\xi^3-3\xi^2+1)\boldsymbol{r}^p+l_0(\xi^3-2\xi^2+\xi)\boldsymbol{n}_x^p\\&+(-2\xi^3+3\xi^2)\boldsymbol{r}^q+l_0(\xi^3-\xi^2)\boldsymbol{n}_x^q.\end{aligned}\tag{57}$$

This interpolation uses the Cartesian position vectors $\boldsymbol{r}^p$, $\boldsymbol{r}^q$ of the nodes and the two tangent vectors $\boldsymbol{n}_x^p$, $\boldsymbol{n}_x^q$ at the nodes, as shown in Fig. 5.

The velocity and acceleration distribution can be found by taking time derivatives as

$$\begin{aligned}\dot{\boldsymbol{r}}(\xi)=&(2\xi^3-3\xi^2+1)\dot{\boldsymbol{r}}^p+l_0(\xi^3-2\xi^2+\xi)\boldsymbol{B}^p\begin{bmatrix}\dot{\lambda}_0^p\\ \dot{\boldsymbol{\lambda}}^p\end{bmatrix}\\&+(-2\xi^3+3\xi^2)\dot{\boldsymbol{r}}^q+l_0(\xi^3-\xi^2)\boldsymbol{B}^q\begin{bmatrix}\dot{\lambda}_0^q\\ \dot{\boldsymbol{\lambda}}^q\end{bmatrix}\end{aligned}\tag{58a}$$

and

$$\begin{aligned}\ddot{\boldsymbol{r}}(\xi)=&(2\xi^3-3\xi^2+1)\ddot{\boldsymbol{r}}^p\\&+l_0(\xi^3-2\xi^2+\xi)\left(\boldsymbol{B}^p\begin{bmatrix}\ddot{\lambda}_0^p\\ \ddot{\boldsymbol{\lambda}}^p\end{bmatrix}+\dot{\boldsymbol{B}}^p\begin{bmatrix}\dot{\lambda}_0^p\\ \dot{\boldsymbol{\lambda}}^p\end{bmatrix}\right)\\&+(-2\xi^3+3\xi^2)\ddot{\boldsymbol{r}}^q+l_0(\xi^3-\xi^2)\left(\boldsymbol{B}^q\begin{bmatrix}\ddot{\lambda}_0^q\\ \ddot{\boldsymbol{\lambda}}^q\end{bmatrix}+\dot{\boldsymbol{B}}^q\begin{bmatrix}\dot{\lambda}_0^q\\ \dot{\boldsymbol{\lambda}}^q\end{bmatrix}\right),\end{aligned}\tag{58b}$$

where

$$\begin{aligned}\boldsymbol{B}^p&=\frac{\partial\boldsymbol{n}_x^p}{\partial(\lambda_0^p,\boldsymbol{\lambda}^{pT})},\quad \dot{\boldsymbol{B}}^p=\frac{\partial\boldsymbol{B}^p}{\partial(\lambda_0^p,\boldsymbol{\lambda}^{pT})}\begin{bmatrix}\dot{\lambda}_0^p\\ \dot{\boldsymbol{\lambda}}^p\end{bmatrix}\\ \boldsymbol{B}^q&=\frac{\partial\boldsymbol{n}_x^q}{\partial(\lambda_0^q,\boldsymbol{\lambda}^{qT})},\quad \dot{\boldsymbol{B}}^q=\frac{\partial\boldsymbol{B}^q}{\partial(\lambda_0^q,\boldsymbol{\lambda}^{qT})}\begin{bmatrix}\dot{\lambda}_0^q\\ \dot{\boldsymbol{\lambda}}^q\end{bmatrix}.\end{aligned}\tag{58c}$$

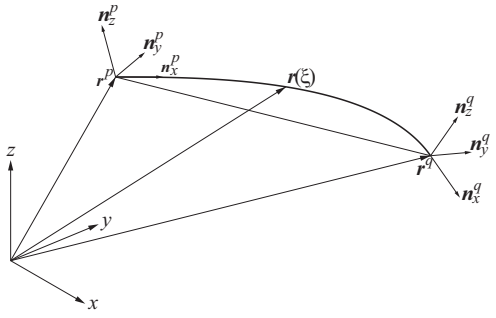

Fig. 5. Configuration of elastic line in the global coordinate system.

3.2. Mass matrix and convective inertia terms

Substitution of Eqs. (58) into Eq. (54) yields the mass matrix

$$\boldsymbol{M}_c=\frac{\rho A l_0}{420}\begin{bmatrix}156\boldsymbol{I} & 22l_0\boldsymbol{B}^p & 54\boldsymbol{I} & -13l_0\boldsymbol{B}^q\\ 22l_0\boldsymbol{B}^{pT} & 4l_0^2\boldsymbol{B}^{pT}\boldsymbol{B}^p & 13l_0\boldsymbol{B}^{pT} & -3l_0^2\boldsymbol{B}^{pT}\boldsymbol{B}^q\\ 54\boldsymbol{I} & 13l_0\boldsymbol{B}^p & 156\boldsymbol{I} & -22l_0\boldsymbol{B}^q\\ -13l_0\boldsymbol{B}^{qT} & -3l_0^2\boldsymbol{B}^{qT}\boldsymbol{B}^p & -22l_0\boldsymbol{B}^{qT} & 4l_0^2\boldsymbol{B}^{qT}\boldsymbol{B}^q\end{bmatrix}\tag{59}$$

and the convective inertia vector

$$\boldsymbol{h}_c=\frac{\rho A l_0}{420}\begin{bmatrix}22l_0\dot{\boldsymbol{B}}^p[\dot{\lambda}_0^p,\dot{\boldsymbol{\lambda}}^{pT}]^T-13l_0\dot{\boldsymbol{B}}^q[\dot{\lambda}_0^q,\dot{\boldsymbol{\lambda}}^{qT}]^T\\ 4l_0^2\boldsymbol{B}^{pT}\dot{\boldsymbol{B}}^p[\dot{\lambda}_0^p,\dot{\boldsymbol{\lambda}}^{pT}]^T-3l_0^2\boldsymbol{B}^{pT}\dot{\boldsymbol{B}}^q[\dot{\lambda}_0^q,\dot{\boldsymbol{\lambda}}^{qT}]^T\\ 13l_0\dot{\boldsymbol{B}}^p[\dot{\lambda}_0^p,\dot{\boldsymbol{\lambda}}^{pT}]^T-22l_0\dot{\boldsymbol{B}}^q[\dot{\lambda}_0^q,\dot{\boldsymbol{\lambda}}^{qT}]^T\\ -3l_0^2\boldsymbol{B}^{qT}\dot{\boldsymbol{B}}^p[\dot{\lambda}_0^p,\dot{\boldsymbol{\lambda}}^{pT}]^T+4l_0^2\boldsymbol{B}^{qT}\dot{\boldsymbol{B}}^q[\dot{\lambda}_0^q,\dot{\boldsymbol{\lambda}}^{qT}]^T\end{bmatrix}.\tag{60}$$

4. Elastic stability

In order to study the vibration properties and the elastic stability we consider small disturbances from an equilibrium configuration $\sigma_i^0\mathcal{D}_{i,k}^0=A_{lk}^0F_l^0$. Substituting Eq. (35) into Eq. (55) and expanding the equations in terms of disturbances $\Delta\boldsymbol{x}$, $\Delta\ddot{\boldsymbol{x}}$ and disregarding second- and higher-order terms yields the linearized equations of motion

$$[\mathcal{D}_{i,k}^0S_{ij}\mathcal{D}_{j,l}^0+\sigma_i^0\mathcal{D}_{i,kl}^0-(A_{mk}F_m)_{,l}^0]\Delta x_l+M_{kl}^0\Delta\ddot{x}_l=0,\tag{61}$$

or in matrix form

$$(\boldsymbol{K}^0+\boldsymbol{G}^0+\boldsymbol{N}^0)\Delta\boldsymbol{x}+\boldsymbol{M}^0\Delta\ddot{\boldsymbol{x}}=\boldsymbol{0}.\tag{62}$$

The matrix $\boldsymbol{K}^0$ is the usual symmetric system stiffness matrix from linear beam theory and $\boldsymbol{G}^0$ is the symmetric geometric stiffness matrix due to the reference load $\boldsymbol{F}^0$ giving rise to reference stress resultants $\boldsymbol{\sigma}^0$. The matrix $\boldsymbol{N}^0$ contains the terms $(A_{mk}F_m)_{,l}^0$ and need not be symmetric.

5. Numerical simulations

For numerical computations, the computer program SPACAR [24] is used. This program can make computations for mechanical systems with interconnected rigid and flexible elements. Specifically, the motion can be simulated for given initial conditions, the equations can be linearized about an arbitrary state of motion, stationary solutions can be determined, and with the linearized equations, eigenfrequencies and corresponding frequency modes as well as the elastic stability can be determined.

5.1. Cantilever beam loaded by a transverse force

As a first example, a cantilever beam loaded by a large transverse tip force is studied (Fig. 6). This example was studied in [16] for the case without shear, which is also studied here to make a comparison. The beam has a length of $L=2$ m, a square cross-section with sides 0.1 m, Young's modulus $E=207$ GPa, and the load is $F=3EI/L^2$, so the deflection would be equal to the length of the beam according to the linear beam theory.

Table 1 shows the tip displacements for different numbers of equal elements. The displacements in the second and third column have been obtained with the modified deformations of Eq. (48), while the displacements in the fourth and fifth column have been obtained with the basic definitions of Eq. (7). The row indicated by ∞ is obtained by extrapolation. The observed rate of convergence is quadratic. This contrasts with the results obtained in [16] where a quartic rate of convergence was obtained, which

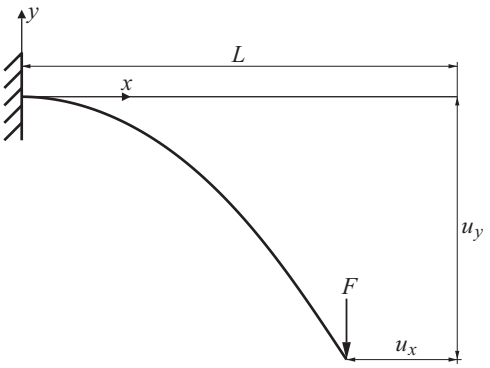

Fig. 6. Cantilever beam loaded by a transverse force.

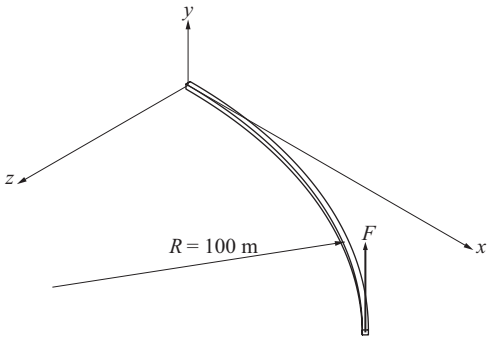

Fig. 7. Cantilever beam initially curved to a 45° arc in the undeformed configuration.

Table 1
Tip displacements; u_x and u_y are obtained with the inclusion of the quadratic terms in the strain definitions, whereas $\hat{u}_x$ and $\hat{u}_y$ lack these terms.

Elements	u_x	u_y	$\hat{u}_x$	$\hat{u}_y$
1	0.901067	1.521304	No conv.	No conv.
2	0.574104	1.276622	0.575338	1.316823
4	0.523295	1.223753	0.521435	1.230945
8	0.512121	1.211296	0.511573	1.212951
16	0.509427	1.208249	0.509285	1.208655
32	0.508759	1.207492	0.508724	1.207593
64	0.508593	1.207303	0.508584	1.207328
128	0.508551	1.207256	0.508549	1.207262
∞	0.508537	1.207240	0.508537	1.207240
∞ [16]	0.508537	1.207240		

can be attributed to the use of a full third-order polynomial interpolation for the displacements. The inclusion of the quadratic terms in the definitions for the generalized deformations gives a small improvement of the computed displacements.

5.2. Cantilever beam initially curved to a 45° arc

An example, originally proposed by Bathe [3], which has recently been considered by Romero [36], consists of a cantilever beam initially curved to an arc of radius 100 m over an angle of 45° in a horizontal plane (Fig. 7). The beam is loaded by a vertical tip force of $F=600$ N. The properties of the beam are $EA = 10\times10^6$ N, $k_{\bar{y}}GA = k_{\bar{z}}GA = 5\times10^6$ N, $k_{\bar{x}}GI_p = EI_{\bar{y}} = EI_{\bar{z}} = 1\times10^7/12$ Nm^2. The beam is modelled by eight equal initially straight beam elements with the nodes on the centre line of the beam. The tip position predicted by the present discrete deformation mode (DDM) formulation, compared with results obtained in the original publication [3], results from several geometrically exact (GE) formulations, from an absolute nodal coordinate formulation (ANCF) [36], a natural coordinate (NC) formulation [2] and a co-rotational (CR) formulation [11] are listed in Table 2. Note that the tip displacement is of the same order of magnitude as the length of the beam.

The results show that all methods provide accurate solutions with the exception of the ANCF solutions. This is even clearer when we compare with ANCF solutions having the same number of degrees of freedom, namely with ANCF (four elements) [36]. The (NC) formulation predicts a larger vertical deflection than those obtained by the other formulations. It is interesting to note that the (DDM) beam model with the basic definitions of Eq. (7) gives a rather accurate result.

Table 2
Tip position (m) for the curved cantilever beam. Initial tip coordinates: 70.71, 0, 29.29 m.

	$F=600$ N		
	r_x	r_y	r_z
Bathe and Belourchi [3]	47.2	53.4	15.9
GE (8 el.) Simo and Vu-Quoc [40]	47.23	53.37	15.79
GE (8 el.) Cardona and Géradin [9]	47.04	53.50	15.56
GE (8 el.) Ibrahimbegović [19]	46.96	53.41	15.69
GE (8 el.) Jelenić and Crisfield [21]	46.97	53.73	15.62
GE (8 el.) Mäkinen [28]	47.01	53.50	15.62
GE (8 el.) Romero [36]	46.98	53.50	15.69
GE (50 el.) Romero [36]	46.89	53.60	15.56
ANCF (4 el.) Romero [36]	59.95	37.55	22.71
ANCF (8 el.) Romero [36]	50.16	50.26	17.16
NC (8 el.) Avello et al. [2]	46.48	54.54	15.26
CR (8 el.) Crisfield [11]	46.84	53.71	15.61
DDM (8 el.) basic def's Eq. (7)	46.95	53.75	15.61
DDM (8 el.) modified def's Eq. (48)	46.94	53.64	15.64
DDM (48 el.) modified def's Eq. (48)	47.14	53.48	15.68

5.3. Lateral buckling of a cantilever beam

In the next example, lateral buckling is considered of a cantilever beam with a narrow rectangular cross-section which is loaded by a transverse force F at its free end in the direction of the larger flexural rigidity, see Fig. 8. The theoretical buckling load is $F_{\text{th}} = 4.013\,599\,344(EIS_t)^{1/2}/l^2$, where EI is the smaller flexural rigidity, S_t is the torsional rigidity and l is the length of the beam. For numerical analysis, the beam is divided in one, two or four equal spatial beam elements. Two cases are considered in Table 3, where $\hat{F}_{\text{cr}}$ are the critical buckling loads which are obtained without the second-order terms and F_{cr} are the critical loads when these terms are included in the analysis.

We observe that with the inclusion of the second-order terms in the bending deformations, the error in the buckling load is decreased by a factor of about three, while the order of convergence remains two. Both approximations converge to the theoretical value.

5.4. Parallel leaf-spring guidance subject to misalignment

A parallel leaf-spring guidance is shown in Fig. 9. It consists of a guided body, the shuttle, supported by two leaf springs. The leaf springs are equal and they are parallel in the reference configuration. The base of the left leaf spring is connected to a hinge, so a torque T_0 or a prescribed misalignment ϕ_0 can be introduced. The stainless steel leaf springs have a thickness $t=0.2$ mm, a

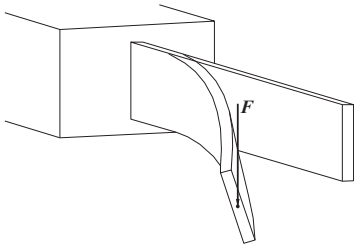

Fig. 8. Lateral buckling of a cantilever beam.

Table 3
Critical loads for lateral buckling of cantilever beam.

Number of elements	F_{cr}/F_{th}	$\hat{F}_{cr}/F_{th}$
1	1.495290	Infinite
2	1.069138	1.220899
4	1.015367	1.046009

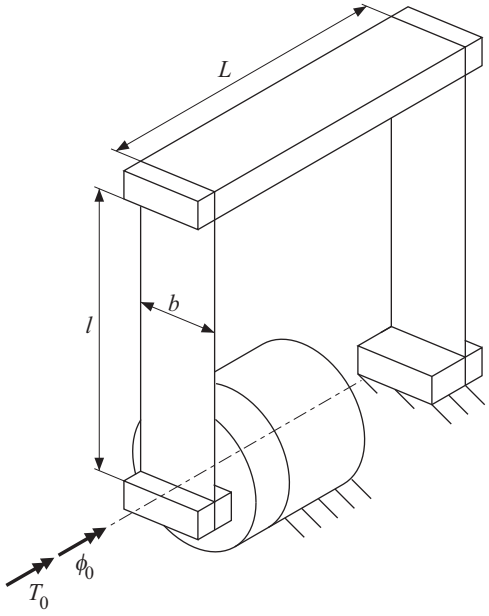

Fig. 9. Parallel leaf-spring guidance with adjustable misalignment.

width $b=30$ mm and a length $l=100$ mm, and they are a distance $L=120$ mm apart. Further details of the model can be found in [31]. Ten spatial beam elements are used to model each leaf spring. The critical torque for buckling is found to be 0.30361 Nm with both the basic definitions of Eq. (7) and the modified definitions of Eq. (48).

The first three natural frequencies as a function of the misalignment angle ϕ_0 are shown in Fig. 10. The three eigenfrequencies drop considerably at the critical angle of about 0.8 milliradians at which bifurcation occurs. The difference between the two formulations is small at zero misalignment, then increases strongly near the critical angle, nearly to a ratio of one to two for the second natural frequency, and then decrease again. It can be observed that the difference for the second natural frequency remains large for angles larger than the critical angle.

6. Conclusions

The paper describes a discrete deformation mode formulation for a three-dimensional shear deformable beam element. The

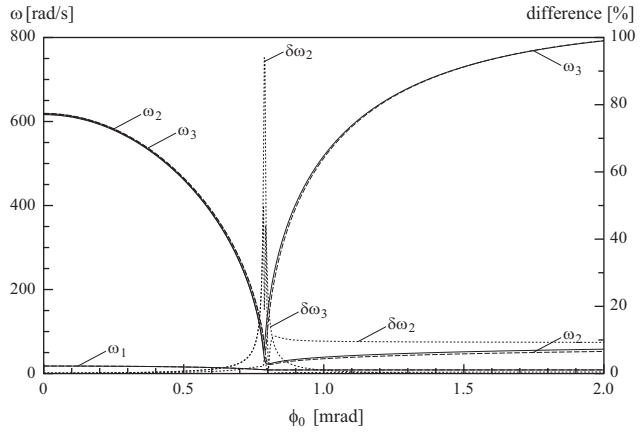

Fig. 10. First three eigenfrequencies for varying misalignments. The solid lines are with the modified definition of (48) and the dashed lines are for the basic definitions of (7). The dotted lines show the relative difference between the eigenfrequencies.

deformation modes are characterized by deformation coordinates, also called generalized deformations, which are related to conventional small-deflection beam theory in a co-rotational frame attached to the element. With the inclusion of additional second-order terms in the definitions of the generalized deformations, a clear separation of axial rigidity and torsion and bending rigidities in two directions is retained, so the deformation modes associated with a large stiffness can be eliminated by constraining them to be zero.

The effect of the second-order terms that accounts for change in configuration is investigated in several examples. It appears that the influence of second-order terms on the displacements is small, except near bifurcation points where load–deflection characteristics change drastically. Furthermore, the use of these terms leads to a modest reduction in the number of elements needed to perform the analysis with the same accuracy. It is demonstrated that highly accurate solutions can be obtained with the present beam finite element formulation.

References

[1] J.H. Argyris, H. Balmer, J.St. Doltsinis, P.C. Dunne, M. Haase, M. Kleiber, G.A. Malejannakis, H.-P. Mlejnek, M. Müller, D.W. Scharpf, Finite element method—the natural approach, Computer Methods in Applied Mechanics and Engineering 17/18 (1979) 1–106.
[2] A. Avello, J. Garcia de Jalon, E. Bayo, Dynamics of flexible multibody systems using Cartesian coordinates and large displacement theory, International Journal for Numerical Methods in Engineering 32 (1991) 1543–1563.
[3] K.-J. Bathe, S. Bolourchi, Large displacement analysis of three-dimensional beam structures, International Journal for Numerical Methods in Engineering 14 (1979) 961–986.
[4] T. Belytschko, L.W. Glaum, Application of higher order co-rotational stretch theories to nonlinear finite element analysis, Computers and Structures 10 (1979) 175–182.
[5] J.F. Besseling, The complete analogy between the matrix equations and the continuous field equations of structural analysis, in: F. Haus (Ed.), International Symposium on Analogue and Digital Techniques Applied to Aeronautics, Proceedings, Presses Académiques Européennes, Bruxelles, 1964, pp. 223–242.
[6] J.F. Besseling, Non-linear analysis of structures by the finite element method as a supplement to a linear analysis, Computer Methods in Applied Mechanics and Engineering 3 (1974) 173–194.
[7] J.F. Besseling, Derivatives of deformation parameters for bar elements and their use in buckling and postbuckling analysis, Computer Methods in Applied Mechanics and Engineering 12 (1977) 97–124.
[8] J.F. Besseling, Non-linear theory for elastic beams and rods and its finite element representation, Computer Methods in Applied Mechanics and Engineering 31 (1982) 205–220.
[9] A. Cardona, M. Géradin, A beam finite element non-linear theory with finite rotations, International Journal for Numerical Methods in Engineering 26 (1988) 2403–2438.

[10] G.R. Cowper, The shear coefficient in Timoshenko's beam theory, ASME Journal of Applied Mechanics 33 (1966) 335–340.
[11] M.A. Crisfield, A consistent co-rotational formulation for non-linear, three-dimensional, beam elements, Computer Methods in Applied Mechanics and Engineering 81 (1990) 131–150.
[12] M.A. Crisfield, G. Jelenić, Objectivity of strain measures in the geometrically exact three-dimensional beam theory and its finite-element implementation, Proceedings of the Royal Society A 455 (1999) 1125–1147.
[13] C.A. Felippa, B. Haugen, A unified formulation of small-strain corotational finite elements: I. Theory, Computer Methods in Applied Mechanics and Engineering 194 (2005) 2285–2335.
[14] M. Géradin, A. Cardona, Flexible Multibody Dynamics: A Finite Element Approach, John Wiley and Sons, Chichester, 2001.
[15] J.M. Gere, S.P. Timoshenko, Mechanics of Materials, PWS, Boston, MA, 1997.
[16] J. Gerstmayr, H. Irschik, On the correct representation of bending and axial deformation in the absolute nodal coordinate formulation with an elastic line approach, Journal of Sound and Vibration 318 (2008) 461–487.
[17] J. Gerstmayr, A. Mikkola, H. Sugiyama, Developments and future outlook of the absolute nodal coordinate formulation, in: Proceedings of the Second Joint International Conference on Multibody System Dynamics, Stuttgart, Germany, May 2012.
[18] K.M. Hsiao, J.Y. Lin, W.Y. Lin, A consistent co-rotational finite element formulation for geometrically nonlinear dynamic analysis of 3-D beams, Computer Methods in Applied Mechanics and Engineering 169 (1999) 1–18.
[19] A. Ibrahimbegović, On finite element implementation of geometrically nonlinear Reissner's beam theory: three-dimensional curved beam elements, Computer Methods in Applied Mechanics and Engineering 122 (1995) 11–26.
[20] M. Iura, S.N. Atluri, Dynamic analysis of planar beams with finite rotations by using inertial and rotating frames, Computers and Structures 55 (1995) 453–462.
[21] G. Jelenić, M.A. Crisfield, Geometrically exact 3D beam theory: implementation of a strain-invariant finite element for statics and dynamics, Computer Methods in Applied Mechanics and Engineering 171 (1999) 141–171.
[22] A. Jennings, Frame analysis including change of geometry, Journal of Structural Division, ASCE 94 (ST3) (1968) 627–644.
[23] J.B. Jonker, A finite element dynamic analysis of spatial mechanisms with flexible links, Computer Methods in Applied Mechanics and Engineering 76 (1989) 17–40.
[24] J.B. Jonker, J.P. Meijaard, SPACAR—computer program for dynamic analysis of flexible spatial mechanisms and manipulators, in: W. Schiehlen (Ed.), Multibody Systems Handbook, Springer-Verlag, Berlin, 1990, pp. 123–143.
[25] J.B. Jonker, J.P. Meijaard, Definition of deformation parameters for beam elements and their use in flexible multibody system analysis, in: Proceedings of the Multibody Dynamics 2009, ECCOMAS Thematic Conference, Warsaw, 2009.
[26] J.B. Kuipers, Quarternions and Rotation Sequences: A Primer with Applications to Orbits, Aerospace and Virtual Reality, Princeton University Press, Princeton, Oxford, 2002.
[27] A.E.H. Love, A Treatise on the Mathematical Theory of Elasticity, Dover, New York, 1944.
[28] J. Mäkinen, Total Lagrangian Reissner's geometrically exact beam element without singularities, International Journal for Numerical Methods in Engineering 70 (2007) 1009–1048.
[29] J.P. Meijaard, Direct determination of periodic solutions of the dynamical equations of flexible mechanisms and manipulators, International Journal for Numerical Methods in Engineering 32 (1991) 1691–1710.
[30] J.P. Meijaard, Validation of flexible beam elements in dynamic programs, Nonlinear Dynamics 9 (1996) 21–36.
[31] J.P. Meijaard, D.M. Brouwer, J.B. Jonker, Analytical and experimental investigation of a parallel leaf spring guidance, Multibody System Dynamics 23 (2010) 77–97.
[32] C. Pacoste, A. Eriksson, Beam elements in instability problems, Computer Methods in Applied Mechanics and Engineering 144 (1997) 163–197.
[33] E. Reissner, On one-dimensional finite-strain beam theory: the plane problem, Journal of Applied Mathematics and Physics (ZAMP) 23 (1972) 795–804.
[34] E. Reissner, On one-dimensional large-displacement finite-strain beam theory, Studies in Applied Mathematics 52 (1973) 87–95.
[35] I. Romero, The interpolation of rotations and its application to finite element models of geometrically exact rods, Computational Mechanics 34 (2004) 121–133.
[36] I. Romero, A Comparison of finite elements for non-linear beams: the absolute nodal coordinate and geometrically exact formulations, Multibody System Dynamics 20 (2008) 51–68.
[37] A.L. Schwab, J.P. Meijaard, Comparison of three-dimensional flexible beam elements for dynamic analysis: classical finite element formulation and absolute nodal coordinate formulation, ASME Journal of Computational and Nonlinear Dynamics 5 (1) (2010) 1–10, Article no. 011010.
[38] A.A. Shabana, R.A. Yakoub, Three dimensional absolute nodal coordinate formulation for beam elements: theory, ASME Journal of Mechanical Design 123 (2001) 606–613.
[39] J.C. Simo, A finite strain beam formulation, the three-dimensional dynamic problem I, Computer Methods in Applied Mechanics and Engineering 49 (1985) 55–70.
[40] J.C. Simo, L. Vu-Quoc, A three-dimensional finite strain rod model. Part II: computational aspects, Computer Methods in Applied Mechanics and Engineering 58 (1986) 79–116.
[41] J.T. Sopanen, A.M. Mikkola, Description of elastic forces in absolute nodal coordinate formulation, Nonlinear Dynamics 34 (2003) 53–74.
[42] H. Sugiyama, J. Gerstmayr, A.A. Shabana, Deformation modes in the finite absolute nodal coordinate formulation, Journal of Sound and Vibration 298 (2006) 1129–1149.
[43] W. Visser, J.F. Besseling, Large Displacement Analysis of Beams, Report WTHD 10, Delft University of Technology, Delft, 1969.
[44] R.A. Yakoub, A.A. Shabana, Three dimensional absolute nodal coordinate formulation for beam elements: implementation and applications, ASME Journal of Mechanical Design 123 (2001) 614–621.
[45] K. van der Werff, J.B. Jonker, Dynamics of flexible mechanisms, in: E.J. Haug (Ed.), Proceedings of Computer Aided Analysis and Optimization of Mechanical System Dynamics, Springer-Verlag, Berlin, 1984, pp. 381–400.